LENS DISTORTION CORRECTION BY ANALYSING THE SHAPE OF PATTERNS IN HOUGH TRANSFORM SPACE

A thesis presented in partial fulfilment of the requirements for the degree of

Master of Engineering

In

Electronics and Computer Engineering

at Massey University, Manawatu, New Zealand

YUAN CHANG

2018

Abstract

Many low cost, wide angle lenses suffer from lens distortion, resulting from a radial variation in the lens magnification. As a result, straight lines, particularly those in the periphery, appear curved. The Hough transform is a commonly used linear feature detection technique within an image. In Hough transform space, straight lines and curved lines have different shapes of peaks. This thesis proposes a lens distortion correction method named SLDC based on analysing the shape of patterns in the Hough transform space. It works by reconstructing the distorted line from significant points on the smile-shaped Hough pattern. It then optimises the distortion parameter by mapping the reconstructed curved line into a straight line and minimising the RMSE. From both simulation and correcting real world images, the SLDC provides encouraging results.

Keywords: Hough transform; barrel lens distortion correction; straight line; shape of peaks

Acknowledgements

Table of Content

List of Figures

List of Tables

Chapter 1 Introduction

In image processing the camera records a digital representation of a scene or object. In many cases, it is important that it is an accurate representation. Unfortunately, a majority of cameras use lenses to collect light and most lenses introduce some form of distortion. Figure 1 shows an example of radial lens distortion.

Figure 1: Real scene and what the camera saw with distortion.

1.1. What is Lens Distortion?

For most computer vision and image processing algorithms, the basic camera model for image formation is the pin-hole camera model. It assumes that each image point is generated as a direct projection of the real-world point through the optical centre of the lens. However, a pin-hole camera model is usually invalid due to optical distortion (Bukhari & Dailey, 2010). Real cameras suffer from lens distortion, especially when using wide-angle or fish-eye lenses. In such cases the problem becomes more serious.

There are generally two components of lens distortion: radial distortion and tangential distortion. Tsai (1987) has demonstrated that the effect of tangential distortion is insignificant in most cases, and can therefore be neglected. Therefore, in this research, we focus only on radial lens distortion. Radial lens distortion is the result of a different magnification in the centre of the image to that at the edges, causing 'points in the image' to deviate in a non-linear fashion from their ideal position of a pin-hole camera model. Barrel and pincushion distortion are two common instances of radial lens distortion. For barrel lens distortion, the image has a higher resolution in the centre of the image than at its periphery while pincushion distortion has the opposite effect. Figure 2 compares the effect of barrel and pincushion lens distortions. One significant feature of radial lens distortion is its symmetry about the centre of distortion and that it does not affect the image at the distortion centre. As the result of radial lens distortion, straight lines, especially those located near the edges of the image, appear curved.
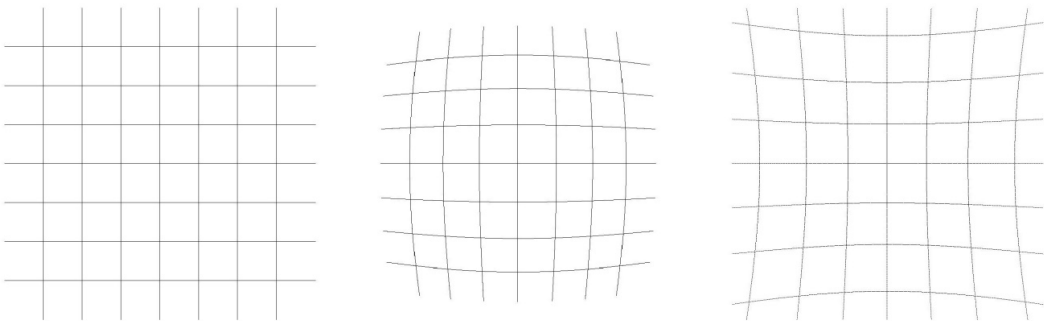
Figure 2: Left: the original grid; Centre: the effect of barrel radial distortion; Right: the effect of pincushion distortion.

In many cases, radial lens distortion can be generally neglected, and it can even be used as an artistic effect. However, for more rigorous image processing tasks or machine vision systems, where measurements are made from the image, lens distortion cannot be accepted. Not only does radial lens distortion make images captured by the camera less visually appealing to the human observer, it is also critical in many applications where shape recognition, localisation, classification and detection are essential (Cuccihiara et al, 2003).

1.2. Camera Calibration

To correct lens distortion, geometric camera calibration is needed. It aims to correct the lens distortion by mapping pixels in the image to those which would be captured using a simple pinhole camera model. The parameters which affect the mapping can be separated into two categories:

External parameters describe the relationship between the camera frame and the world frame, including position and orientation.

Internal parameters describe the characteristic of the camera, and include the lens focal length, pixel scale factors, and location of the optical centre within the image. The distortion parameters which describe the geometric nonlinearities of the camera also belong to this category.

The internal and external parameters (apart from lens distortion) can be grouped into a single 3×4 perspective transformation matrix (Xu, et al, 2006) . These parameters require accurate knowledge of 3D to 2D point correspondence to determine their values. The lens distortion parameters are simpler in that they are modelled entirely in 2D image space.

There are three categories of geometric camera calibration methods based on the features used (Furukawa & Shinagawa, 2003) (Devernay & Faugeras, 1995). The first approach uses feature points, consisting of dots, circles or corners which can be easily extracted from an image of a calibration grid (Duane, 1971). After identifying the feature points, the calibration method finds the best camera-external and internal parameters that relate the position of the 3D points

to the measured feature points in the image (Frederic, et al, 2001). A disadvantage of this approach is that there is coupling between internal and external parameters, which can reduce the accuracy when computing the external and internal parameters at the same time.

The second approach is linear feature based (Lee, et al, 2011) (Wang, et al, 2009) (Strand & Hayman, 2005) (Prescott & McLean, 1997), where the features are one or more straight lines or edges, either from a calibration grid or naturally occurring in the scene. This method assumes that linear features without distortion should be straight, thus, this principle can be used for camera calibration.

There is also a third group of methods which do not need any kind of known calibration points. These are also called auto-calibration methods (Frederic, et al, 1995). They do not depend on the calibration reference object and are unrelated to the scene and camera movements, only making use of the self-constraints of camera internal parameters. Their main disadvantage, is that if all the camera parameters are unknown, they can be very unstable (Frederic, et al, 2001).

The lens distortion correction method explored in this thesis is linear feature based. The linear approach requires some form of edge or line detection method. The next section reviews edge and line detection methods.

1.3. Edge and Line Detection

Since edge or line detection is the initial step for linear feature based lens distortion correction, the accuracy of estimating the lens distortion parameters highly relies on effectively detecting edges and lines. Edges are characterised by step changes in pixel value. Therefore, the most common method to detect edges is gradient based, locating the local extrema in the first derivative of the image.

The Sobel filter (Rafael, et al, 2002) consists of a pair of 3×3 convolution kernels as shown in Figure 3.

-1	0	+1
-2	0	+2
-1	0	+1

Gx

+1	+2	+1
0	0	0
-1	-2	-1

Gy

Figure 3: Convolution kernels used by the Sobel filter

These two kernels are designed to respond maximally to vertical and horizontal edges, one kernel for each of the two perpendicular orientations. The outputs of the filter can be combined together to find the absolute magnitude of the gradient at each point and the orientation of that gradient.

The Prewitt filter (Maini & Aggarwal, 2009) has the kernels shown in Figure 4. These are similar to the Sobel filter kernels, and are used in a similar way.

-1	0	+1
-1	0	+1
-1	0	+1

Gx

+1	+1	+1
0	0	0
-1	-1	-1

Gy

Figure 4: Convolution kernels used by the Prewitt filter

A more powerful edge detection method is the Canny edge detection algorithm (Canny, 1987). Compared to the first two methods, it is more robust to with respect to noise. The Canny edge detector first smooths the image with a Gaussian filter to reduce noise. The next step is to determine edge strength and orientation by taking the gradient of the image using a Sobel filter. The edge is thinned by supressing the non-maximum gradients perpendicular to the edge. Edges are detected using hysteresis based thresholding to select strong edges, along with connected weaker edges. The Canny detector has improved signal to noise ratio and better detection accuracy especially in noise conditions than the simple Sobel or Prewitt filters on their own. However, it requires complex computation and is time-consuming.

After edge detection the Hough transform is a reliable way to detect linear features (Bukhari & Dailey, 2010). The Hough transform works by converting the original image into a parameter space, referred to as the Hough space. Each point in Image space 'votes' in Hough transform space for the parameters of all lines consistent with that point. A line in image space results in multiple votes at the point in Hough transform space corresponding to the line's parameters. By finding the local maxima (peaks) in parameter space, it is possible to locate the dominant lines in the original image. In the Hough transform space, straight lines and curved lines yield different shaped peaks.

A straight line in the image gives a peak in the Hough transform space concentrated at a point. A curved line yields a more 'spread out' pattern because the curvature cannot be represented by a single set of line parameters. These are illustrated in Figure 5. In this research, we assume there is a relationship between the shape of the blurred peak and the lens distortion. Accordingly, a lens distortion correction method based on analysing the shape of peaks in Hough transform space is proposed.
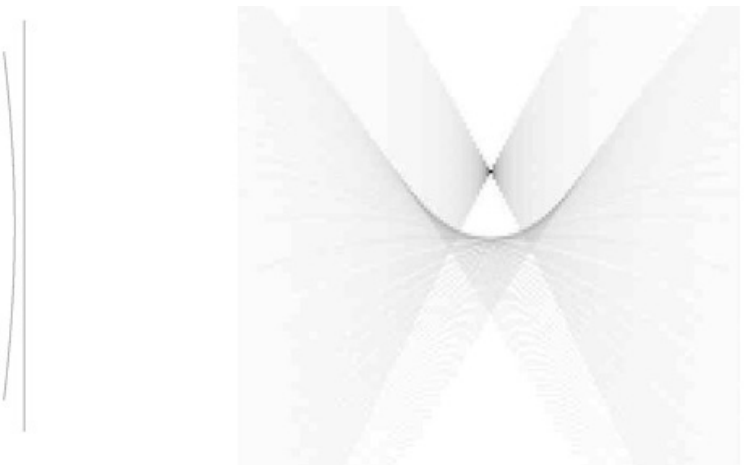
Figure 5: Left: a straight line and that line curved by lens distortion; Right: the corresponding peaks in the Hough space.

1.4. Research Goals

To explore how the shape of the peaks in the Hough transform can be used to estimate lens distortion parameters. This requires analysing how lens distortion affects the peak shape, and identifying features of the peak pattern that can be used to calculate the distortion parameters. A second goal is to investigate the accuracy of the parameter estimation, and identify the factors that limit the accuracy.

1.5. Overview

This thesis is organised as follows. Chapter 2 reviews lens distortion models and the Hough transform. Chapter 3 analyses the shape of peaks in the Hough transform space and investigates the relationships between the distortion in image space and the shape of the Hough pattern. In Chapter 4 the basic steps of our method are presented. An accuracy study of the correction method is presented in Chapter 5. Discussions and examples of correcting real-world images are covered in Chapter 6. Chapter 7 provides the conclusion and suggestions for future research.

Chapter 2 Background

2.1. Modelling Lens Distortion

In digital image processing and computer vision, the most basic camera model is the pin-hole camera model (Tsai, 1987). It assumes that each image point is generated as a direct projection of a real-world point through the optical centre (Cucchiara et al., 2003). The pin-hole camera model maps a three-dimensional point P whose coordinates in the camera-centred coordinate system are (X, Y, Z) to an image point $p = (x, y)$ on the image plane:

$$x = f\frac{X}{Z}$$
$$y = f\frac{Y}{Z}$$

$$(1)$$

where f is the effective focal length of the camera.

However, due to the effects of lens distortion, real cameras rarely follow the pin-hole model. Therefore, the pin-hole model is not satisfactory for a real camera (Mohr & Triggs, 1996). Since lens distortion is predominantly radial, a general radial Taylor series model of distortion has been proposed (McGlone, et al, 1980). Given a 'distorted' image point $p_d = (x_d, y_d)$, the 'undistorted' image point $p_u = (x_u, y_u)$ can be obtained as follows:

$$x_u = c_x + (x_d - c_x)(1 + \kappa_1 r_d^2 + \kappa_2 r_d^4 + \cdots)+\dots$$
$$p_1[2(x_d - c_x) + r_d^2] + 2p_2(x_d - c_x)(y_d - c_y)$$

$$(2)$$

$$y_u = c_y + (y_d - c_y)(1 + \kappa_1 r_d^2 + \kappa_2 r_d^4 + \cdots)+\dots$$
$$p_1[2(y_d - c_y) + r_d^2] + 2p_2(x_d - c_x)(y_d - c_y)$$

$$(3)$$

where (c_x, c_y) are the coordinates of the centre of distortion, and $r_d = \sqrt{(x_d - c_x)^2 + (y_d - c_y)^2}$, κ_1 and κ_2 are the radial lens Taylor series coefficients, and p_1, p_2 are the tangential Taylor series coefficients. Tsai (1987) noted that the tangential distortion can be neglected. This was demonstrated experimentally by Li & Lavest (1996), and in many cases, only one or two radial coefficients are sufficient.

$$\begin{cases} x_u = c_x + (x_d - c_x)(1 + \kappa_1 r_d^2 + \kappa_2 r_d^4 + \cdots) \\ y_u = c_y + (y_d - c_y)(1 + \kappa_1 r_d^2 + \kappa_2 r_d^4 + \cdots) \end{cases}$$

$$(4)$$

2.1.1. Polynomial Lens Distortion Models

The standard model for radial lens distortion is an odd polynomial is

$$r_d = f(r_u) \tag{5}$$

where r_d is the radius of a point in the distorted image, and r_u is the distance of the corresponding point in the original undistorted image (both relative to the centre of distortion). Unlike (4), equation (5) is a forward model of the lens distortion correction, which maps points from the undistorted image to the distorted one.

Odd Polynomial Model

In image processing and computer vision tasks the most commonly used distortion model is the polynomial distortion model, based on a Taylor series expansion. Generally, an odd model can represent lens distortion while maintaining radial symmetry:

$$r_d = r_u + \kappa_1 r_u^3 + \kappa_2 r_u^5 + \kappa_3 r_u^7 + \cdots \tag{6}$$

where κ_i are the radial lens distortion coefficients (note these coefficients differ from those in (4)).

The "perfect" approximation would be a polynomial of infinite degrees; however, this is not necessary. Researchers and measurements demonstrate that for typical camera lenses, a low order approximation is sufficient and more terms only cause numerical instability (Tsai,1980). According to Faugeras and Toscani (1987) the first order component corrects more than 90% of the radial distortion. Beyer (1992) also showed that using only the first-order radial distortion model could achieve an accuracy of about 0.1 pixels in image space using lenses exhibiting large distortion.

A disadvantage of polynomial models is that they are hard to invert, and in general there is no analytic inverse. Therefore an approximation must be used.

Mallon and Whelan (2004) presented an approximate inverse model of this polynomial model with (two distortion coefficients).

$$r_u = r_d - r_d \left(\frac{\kappa_1 r_d^2 + \kappa_2 r_d^4 + \kappa_1^2 r_d^4 + \kappa_2^2 r_d^8 + 2\kappa_1 \kappa_2 r_d^6}{1 + 4\kappa_1 r_d^2 + 6\kappa_2 r_d^4} \right) \tag{7}$$

In this research only a first order distortion model was considered. We assume that this is a sufficient approximation for mild to moderate distortion.

$$r_d \approx r_u + \kappa_1 r_u^3 = r_u(1 + \kappa_1 r_u^2) \tag{8}$$

The distorted coordinates are given by the formula:

$$x_d = x_u(1 + \kappa_1 r_u^2)$$
$$y_d = y_u(1 + \kappa_1 r_u^2)$$

(9)

Generally, for correction we want $r_d = f(r_u)$. So that we can determine where each point in our corrected image (x_u, y_u) comes from the distorted image (x_d, y_d). The simplified version of equation (7) for a first order distortion model is, given by setting $\kappa_2 = 0$.

$$r_u \approx r_d - r_d \left(\frac{\kappa_1 r_d^2 + \kappa_1^2 r_d^4}{1 + 4\kappa_1 r_d^2} \right)$$

(10)

This decreases the accuracy of this model. However, from simulation the approximate model (10) provides an acceptable accuracy. Figure 6 shows the error introduced after distortion using (8) and correction using (10), the RMS error was less than half pixel, even with serious distortion (In Figure 6 the RMSE in the highlight corner is higher than half pixel). Since the serious error only occur in the corners of the image ($r > 0.85$) for severe distortion ($\kappa_1 > 0.06$), the approximation model is sufficient for general lens distortion except for distortion from fish-eye lenses.
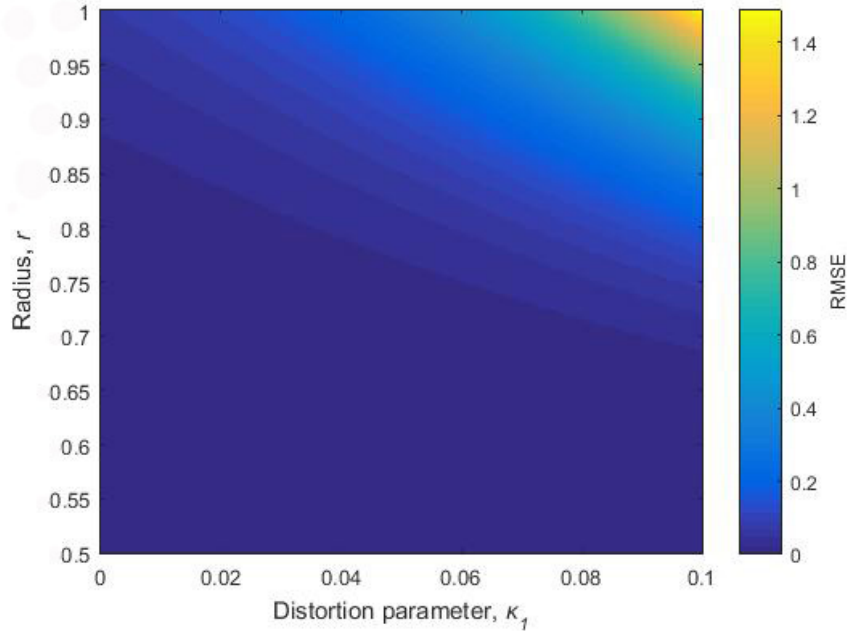
Figure 6: Error of approximate inverse model as a function of distortion parameter κ_1 and normalised radius from image centre.

The Division Model

Fitzgibbon (2001) introduced the division model as it can more accurately represent severe distortion with fewer parameters.

$$r_u = \frac{r_d}{1 + \sum_{n=1}^{\infty} \kappa_n r_d^{2n}}$$
$$= \frac{r_d}{1 + \kappa_1 r_d^2 + \cdots + \kappa_n r_d^{2n} + \cdots} \tag{11}$$

Even though this model looks similar to the standard polynomial model it is not the inversion of it. The parameters in (11) are different from those in (6). The parameter for the first order version of this model can be determined by circle fitting (Barreto & Daniilidis, 2005).

Modelling Fisheye Lens

Unlike regular lenses, the fisheye and wide-angle lenses cannot be described adequately by a low order polynomial model. According to Shah and Aggarwal (1996) considerable distortion remains even with seventh order components. So in their model they used both odd and even components to describe the lens distortion of the fisheye lens.

$$r_d = \sum_{n=1}^{\infty} \kappa_n r_u^n = \kappa_1 r_u^1 + \cdots + \kappa_n r_u^n + \cdots \tag{12}$$

A similar model which has the zero order component was given by Basu and Licardie (1995).

$$r_d = \kappa_0 + \kappa_1 r_u^1 + \cdots + \kappa_n r_u^n + \cdots \tag{13}$$

2.1.2. Non-Polynomial Models of Radial Distortion

The polynomial lens distortion model suffers a common limitation: it is hard to invert. The most significant advantage of non-polynomial models is they are more readily inverted analytically (Hughes, et al, 2008).

The Fish-Eye Transform

Basu and Licardie (1995) proposed the fish-eye transform based on the observation that a fish-eye image has higher resolution in the centre areas and the resolution decreases toward the edge of the image:

$$r_d = s \ln(1 + \lambda r_u) \tag{14}$$

Where s is a simple scalar and λ controls the level of distortion within the image.

The inverse of this model can be written as:

$$r_u = \frac{e^{\frac{r_d}{s}} - 1}{\lambda}$$

(15)

The Field View Model

Devernay and Faugeras (2001) described the field-of-view model, based on a simple optical model of a fish-eye lens:

$$r_d = \frac{1}{\omega} \arctan\left(2r_u \tan\frac{\omega}{2}\right)$$

(16)

Where ω is the angular field-of-view of the ideal fish-eye camera.

The inverse of this model is:

$$r_d = \frac{\tan(r_d\omega)}{2\tan\frac{\omega}{2}}$$

(17)

Perspective Model

Another frequently used model for radial distortion is the perspective model (Ishii et al, 2003):

$$r_d = f\arctan\left(\frac{r_u}{f}\right)$$

(18)

where f is the apparent focal length of the fish-eye camera The inverse of this model is:

$$r_u = f\tan\left(\frac{r_d}{f}\right)$$

(19)

Apart from being easier to analytically invert, and being better at modelling fisheye distortion, the non-polynomial models do not give a significant advantage for regular lenses.

This section has reviewed both polynomial and non-polynomial models of lens distortion, including models of fish-eye and wide-angle lenses. However, there are many different models which are not mentioned in this review. This research is based on the first odder odd polynomial model, which is adequate for correcting standard lenses with low to moderate distortion.

2.2. Hough Transform

The Hough transform is a feature extraction technique used in image analysis, computer vision, and digital image processing. It has long been used to detect lines and other parameterised shapes within an image. The idea of the Hough transform is to transform the information within an image into a parameter space, and to analyse the parameter space instead of the original image. The original Hough transform was initially invented for machine analysis of bubble

17

chamber photographs by Hough in 1959. The original Hough transform (Hough, 1959) uses the slope and intercept of straight lines in original space to create the parameter space. In the pixel domain a straight line can be represented as:

$$y = mx + c \tag{20}$$

We assume (x_1, y_1) is a point on the straight line, and for this point in equation (20) m and c (which are the slope and intercept) are parameters of the line. If we rewrite equation (20) as function of x_1 and y_1:

$$c = -x_1 m + y_1 \tag{21}$$

Then this represents the relationship between the parameters for all lines that pass through (x_1, y_1). In the 'mc' parameter space, (21) appears as a straight line. Point (x_1, y_1) votes for all points in parameter space according to (21). These votes represent sets of parameters that are compatible with (x_1, y_1). Another point within 'xy' image space (x_2, y_2), creates another straight line in 'mc' space. Because these two points define a straight line, the parameter lines of these two points intersect in 'mc' space at the parameters corresponding to the slope and intercept of the line connecting these two points (see Figure 7).
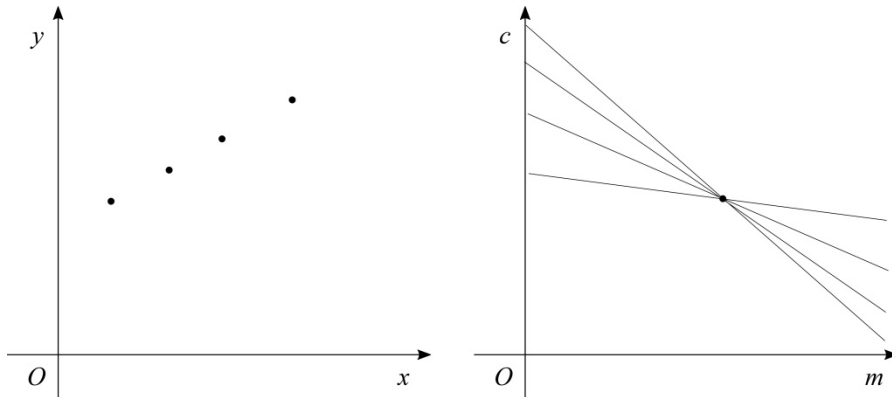
Figure 7: Original Hough transform

Multiple collinear points in 'xy' space result in multiple votes for the line consistent with the data, and therefore produce a peak. By detecting the local maximum (the peak) we can find the parameters of the original straight line within 'xy' space. The Hough transform converts the problem of identifying line patterns in an image into its dual problem of detecting local maxima in Hough parameter space. However, a limitation of the original Hough transform, for equation (20) is that the slope and intercept become very large as the line approaches vertical. This problem can be solved by using two sets of parameter space (Hough, 1962), one for the horizontal lines and one for vertical lines.

$$c_1 = -m_1 x_i + y_i \quad (-1 \leq m_1 \leq 1)$$
$$c_2 = -m_2 y_i + x_i \quad (-1 \leq m_2 \leq 1) \tag{22}$$

To overcome this limitation, Duda and Hart (1972) proposed the rho-theta parametrization of lines:

$$\rho = x \cos \theta + y \sin \theta \tag{23}$$

where ρ is the distance from the origin to the closest point on the line and θ is the angle between the x axis and the line connecting the origin with that closest point (see Figure 8). This has now become the standard Hough transform.
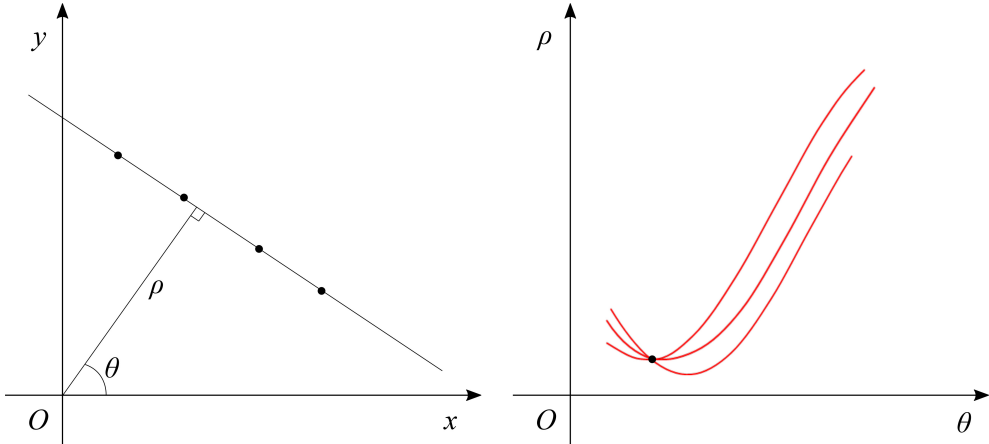
Figure 8: Standard Hough transform.

The standard Hough transform represents every possible line that a point in the 'xy' space as a sinusoidal curve in '$\rho\theta$' Hough space. Equation (23) therefore defines the set of votes cast by an edge point. In other words, an edge point in image space votes for combinations of parameters it is compatible with. If points in 'xy' space belong to a straight line, their corresponding curves in Hough space intersect in '$\rho\theta$' space at the point corresponding to the parameters of that line (see Figure 8). Compared to other points in the parameter space, the number of sinusoidal traces which pass through the intersection is higher, resulting in more votes. Peaks in parameter space therefore indicate the parameters of lines which have significant support in the original image. As with the original Hough transform, if the line in image space is curved by radial lens distortion, in Hough space the peak corresponding to the line will be blurred. However, in this research, we choose to analyse the shape of the pattern around the peak using the original Hough transform, because straight lines are easier to analyse than sinusoidal traces.

Although the Hough transform is a popular tool for line detection, it suffers from high computational cost. To solve this problem and make the Hough transform more suitable for real time applications, the gradient Hough transform was introduced. The gradient Hough transform measures the orientation of the edge and rather than voting for all possible lines through that point, it only votes for a small range of angles (or slopes in the original Hough transform) (Fernandes & Oliveira, 2008). In addition to reducing the computation, it is also makes locating the peaks easier because it reduces the background clutter from irrelevant votes.

2.3. Related Work

Few works have investigated the use of the Hough transform for camera lens distortion correction. Cucchiara *et al* (2003) introduced a Hough transform based measurement tool to indicate line straightness. They adjusted the radial lens distortion parameter to maximise the votes in the Hough transform of the corrected image, at the parameters corresponding to a single straight line in image space. They apply the correction to the image and then take the Hough transform. Their method can be separated into two steps; first they extract the linear feature for analysis, and then estimate the distortion parameter. For the first step, the authors developed an automatic region of interest finding procedure. However, it only works with horizontal or vertical lines; for more general cases, the linear feature needs to be found manually. Once the linear feature is extracted from the image, the authors adjust the distortion parameter to maximize the maximal vote from the corrected image. This method can work with a single image which contains a curved line, or a video with multiple frames. However, the precision depends on the resolution within Hough space. In this work, the authors assume that the centre of the distortion is in the centre of the image. When estimating the lens distortion parameter only one curved line was used which limits the accuracy of this method.

Flores *et al* (2014) presented a two steps correction method. First, they obtain an initial approximation of the distortion parameter by embedding the radial distortion parameter into the Hough parameter space. By maximizing the votes and the distance from line segment to the origin, the longest distorted line and the initial approximation distortion parameter can be optimized. Then, the lens distortion parameter is estimated by minimizing the average of the square of the distance from the corrected primitive points to a straight line. The distortion centre is assumed to be the centre of the image.

Lee *et al* (2011) extended this by making the observation that concentrating the votes at a point in Hough space reduces the entropy. Therefore, by selecting the lens distortion parameter which minimises the entropy of the Hough transform, they were able to take into account all lines in the image. To avoid degeneracy of the entropy caused by the interaction in Hough space between multiple lines, each detected point only votes for a single Hough point based on the estimated image gradient. This method does not require manual selection of a curve and can estimate the distortion parameters independently of the particular distortion model used. Lee et al (2013) then developed this method by adding a focal length estimation approach which made this correction be effective to correct zoom lenses in real time applications.

Edward & Rohan (2009) introduced a 1D Hough transform entropy based correction method. Like Cucchiara *et al*, they extract a single distorted line form the image. The line is parametrised by its orientation with the 1D Hough transform effectively reducing to an orientation histogram. A straight line appears with a single column in the Hough histogram, while a curve is more spread out. By optimizing the distortion parameter to minimize the entropy of the corresponding normalized histogram, the distortion parameter can be estimated. Kunina *et al* (2017)

developed this method by using the fast Hough transform, which enable this method to correct distortion from a sequence of video frames.

These previous methods only use the Hough transform to determine if the line in the corrected image are straight. They do not derive the lens distortion parameter from the Hough transform.

Detecting curved lines (distorted straight lines) is not trivial, especially in the case of large distortion. For this reason, many correction methods require locating the curves manually. Although the Hough transform is powerful for detecting straight lines, when the line is curved by lens distortion the Hough transform can fail to detect it, because the points on the curve do not vote for the same set of line parameters. Aleman-Flores *et al* (2014) proposed a line detection and lens distortion correction method, by introducing a third parameter to the Hough transform which represents the lens distortion. For each value of the distortion parameter (using a first order model), the edge pixels vote using a gradient Hough transform. The distortion parameter with the strongest votes provides an initial estimate of the distortion, and enables the curved line to be detected reliably. However, because of coarse quantisation, the distortion parameter estimated from Hough transform is not accurate enough to be used directly. A second order model is fitted using the detected curved lines, initialised using the estimate from the Hough transform.

Cai and Miklavcic (2013) presented an automatic curve selection method in the context of lens distortion correction based on the Hough transform energy. The energy defines how concentred the peak is in Hough space. For a detected edge in the image space, if their corresponding points in the Hough space all located at a small range, this edge will be selected as a curved line. Then the distortion parameter (κ) can be estimated by adjusting κ to maximise the Hough energy. The authors realized the Hough pattern corresponding to a curved line is separated out compared to that of a straight line. However, they did not analyse the shape of the Hough pattern directly.

In previous works, the authors all used the Hough transform to correct the lens distortion. However, none of them analysed the shape of peaks in the Hough space of the distorted image to estimate the distortion parameters. Furukawa and Shinagawa (2003) analysed the shape of the peak in the Hough space for accurate and robust line segment extraction. They used the shape of the peak patterns around the peak to identify the endpoints of the line segment in the image. Their work inspired us to use the shape of the peaks to directly estimate the lens distortion parameter.

By analysing the shape of patterns around peaks within the parameter space, it should be possible to gather the information about the curved line. By using this information, it should be possible to correct the lens distortion and bring the original straight line back. In the next Chapter, the shape of the Hough pattern will be analysed, and based on the analysis a lens distortion correction method will be presented.

Chapter 3 Analysis of the Shape of Hough Patterns

In this chapter, the shape of patterns in the Hough transform space is analysed as a function of the distortion of lines. We start our analysis with a simplified case, where the line in image space is symmetrical about the origin.

3.1. Straight Line

First, the shape of the pattern in the Hough domain corresponding to a straight line in the image domain will be analysed. This analysis is based on the original Hough transform (parameterised by $y = mx + c$).
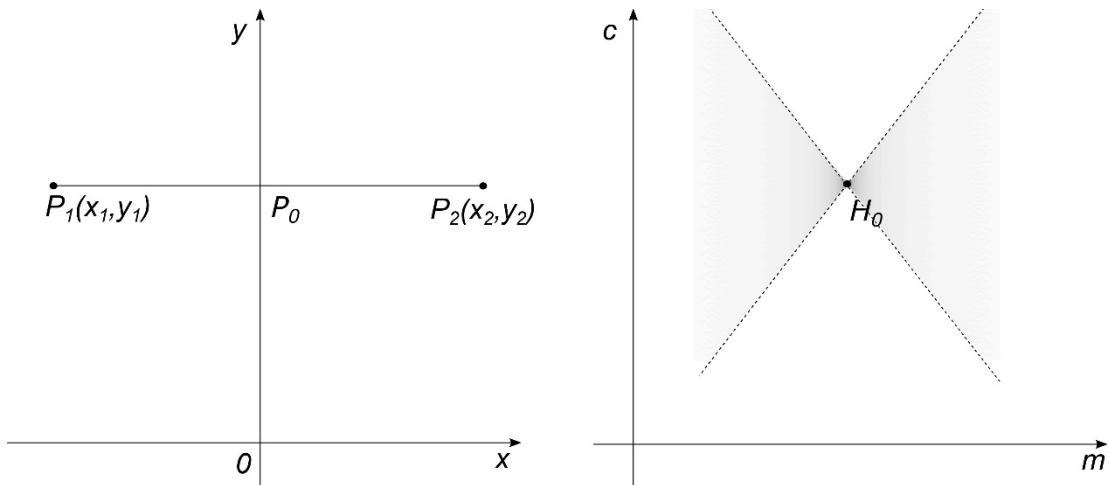
Figure 9: Left: a straight line segment in the image domain; Right: the corresponding pattern in the Hough transform space.

Figure 9 shows a straight line segment with end points P_1 and P_2. We define this straight line as $y = y_0$, where y_0 is the distance from that line to the origin. The line interests the y axis at P_0. The pattern in the Hough transform space resulting from the voting process appears as shown in the right of Figure 9. For a straight line segment, its corresponding pattern of votes will be concentrated at a point (H_0) in the Hough domain. The number of votes received by point H_0 is equal to the number of detected pixels of the original line segment, which makes it significant compared with other nearby points. H_0 should be at $(0, P_0)$ in (m, c) coordinates, the 'c' value (intercept) of point H_0 is equal to the length of $\overline{OP_0}$ in the image space. The two dotted lines along the edges of the Hough pattern correspond to the locus of parameters voted for by the end points of the line segment.

3.2. Curved Line

When the line is curved (for example by lens distortion), the votes are no longer concentrated at a single point in the Hough transform space. Instead there will be a 'blurred' peak, because

the curved line cannot be represented by a single set of parameters. Figure 10 shows the curved line and the corresponding pattern in the Hough transform space (please note the dashed line of Figure 10 is not the same line as the solid line in Figure 9).
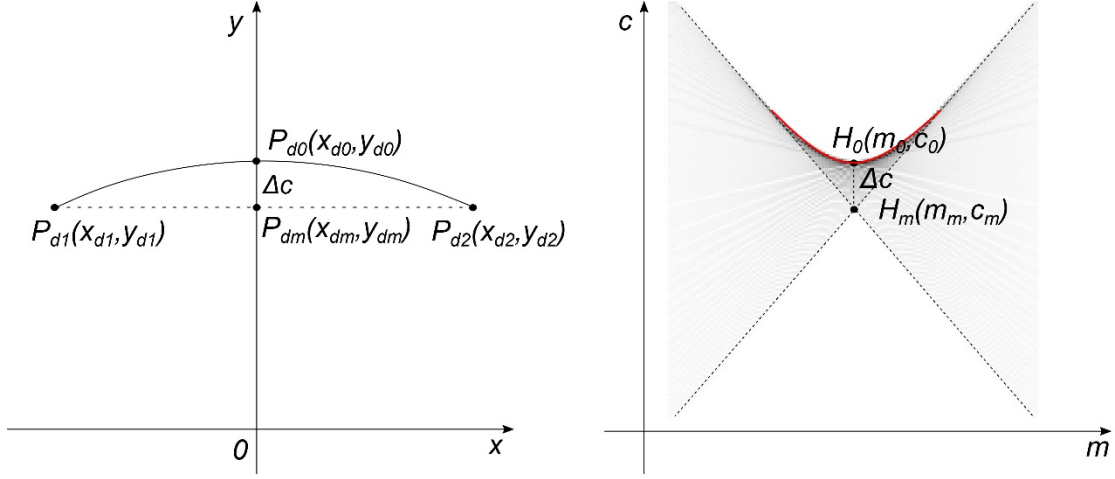
Figure 10: Left: curved line; Right: the corresponding Hough pattern.

3.2.1. The Shape of the 'Blurred' Peak

In Figure 10, points P_{d1} and P_{d2} are the end points of the curved line segment. As with the straight segment, the locus of votes from the endpoints bound the pattern in Hough space. Their intersection H_m, corresponds to the dotted straight line $\overline{P_{d1}P_{d2}}$. The curvature of the distorted line displaces the peak of the votes, and the changing orientation along the line (the tangent) spreads the peak out along the m axis. Each tangent line receives multiple votes, giving a locus of significant points on the upper edge of the Hough pattern (the red curve). We name this locus of significant points as 'smile' because of its shape. The 'smile' ends where the locus becomes straight, in other words when the slope of the locus is equal to the slope of the straight Hough pattern edge corresponding to the tangents to the curve at the endpoints.

On the 'smile' point H_0 is the minimum point, and corresponds to the tangent the curved line at $x = 0$. When the original line segment is horizontal and symmetric about the centre of image, H_0 corresponds to the tangent at point P_{d0} in the left of Figure 10.

The distance between H_0 and H_m is equal to Δc. In the image space, Δc can be represented as:

$$\Delta c = y_{d0} - y_{dm} \tag{24}$$

From the forward lens distortion model:

$$y_{d0} = y_0(1 - \kappa y_0^2) \tag{25}$$

where y_0 is the distance of the original straight from the origin, and:

$$y_{dm} = y_0(1 - \kappa(x_{u1}^2 + y_0^2))$$ (26)

where x_{u1} is the x coordinate of one of the end points of the original line.

If the length of the original line segment is L ($L = x_{u2} - x_{u1}$, or for symmetrical lines $L = 2x_{u2}$), Then substituting (25) and (26) into (24) gives:

$$\Delta c = \kappa y_0 \left(\frac{L}{2}\right)^2$$ (27)

Δc represents how much the Hough pattern is spread out. From (27) there are three factors which influence the shape of the Hough patterns: the amount of lens distortion κ, the distance of the line from the centre of distortion y_0, and the length of the line L. For more general cases where the line segment is not aligned with the axis and not symmetrical about the origin, these three parameters still have a similar influence on the shape of the Hough pattern. The symmetry of the pattern is also affected by the symmetry of the line relative to the centre of distortion.

Figure 11, illustrates the influence of these four factors on the shape of the Hough pattern. Each figure has one different feature compared to Figure 10.

A smaller lens distortion parameter creates a curved line with less distortion, and results in a more compact Hough pattern (See figure 11(a)). The lens distortion parameter has only a slight influence on the slope of the edges of the Hough pattern.

Similarly, when the line segment is closer to the image centre (smaller y_0), the effect of lens distortion becomes less significant. Consequently, the Hough pattern appears contracted. However, the pattern shifts closer to the origin in Hough space corresponding to the change of y_0. Changing y_0 has only a slight influence on the slope of the edges of the Hough pattern, because the influence on the endpoints of the curved line is insignificant.

A shorter line segment brings the end points of the curved line closer to each other, making the slope of the edges of Hough pattern flatter. This flatter pattern is also narrower (the range of tangent slopes is less for a shorter line).

An asymmetric original line segment creates an asymmetric Hough pattern with the curve endpoints giving different slopes for the pattern bounding lines depending on their x coordinates ($c = y - mx$). This asymmetry also makes the 'smile' slanted.

(a) Less distortion parameter

(b) Shorter distance from origin

(c) Shorter line segment

(d) Asymmetric line segment
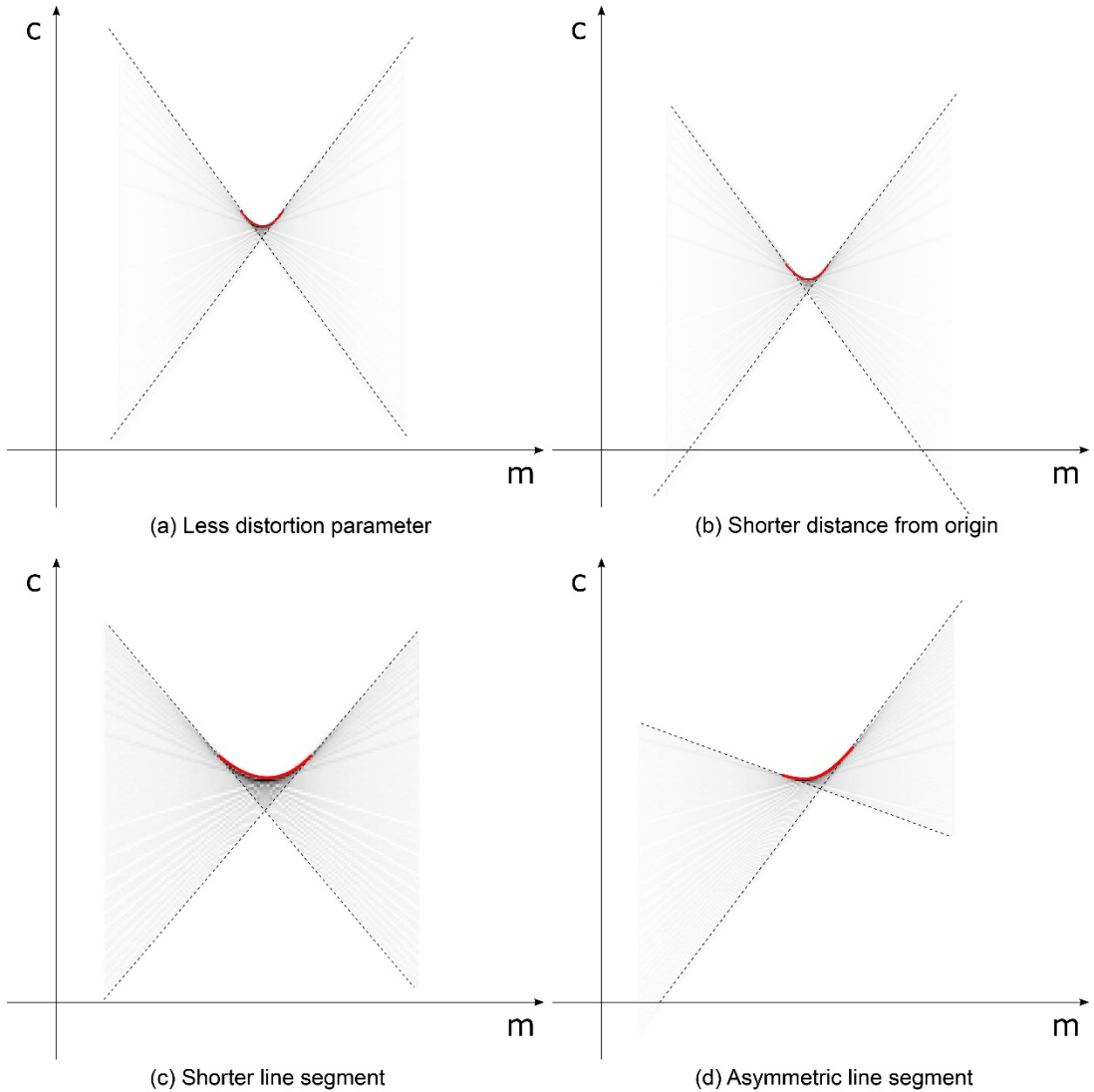
Figure 11: Shape of Hough patterns with different factors relative to Figure 10, (a) has a smaller κ, (b) the straight line is closer to the origin (smaller y_0), in (c) the straight line is shorter (smaller L), and (d) the straight line is asymmetric about the origin

3.2.2. The Slope of the 'Smile'

The curvature of the 'smile' is caused by the changing slope of the distorted line in the image domain. Therefore, the shape of the 'smile' is closely related to the shape of the distorted line, making it important for analysing distortion. Consider point H_1 on the smile (see figure 12).

$H_1(M_1, C_1)$
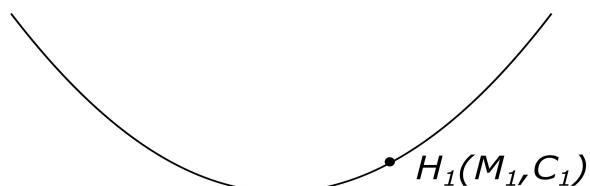
Figure 12: A point on the 'smile' in the Hough pattern

Since $c_1 = y - m_1 x$, this defines a line in image space, this can be constrained further by considering the slope of the smile at H_1:

$$\frac{dc}{dm} = -x \tag{28}$$

For every point on the 'smile' if the parameters of the point and the slope of the 'smile' at that point are known, the coordinates of their corresponding point in the image domain can be estimated. For the two straight edges of the Hough pattern, their slope is equal to the x coordinate of the two end points of the original line.

3.3. Distortion Correction

Based on the shape of the Hough pattern and the relation between the shape and the distorted line, two approaches to lens distortion correction have been designed.

3.3.1. Feature Points Based Method

The first approach is based on locating key feature points of the Hough pattern. To calculate the lens distortion parameter, it is necessary to locate at least 3 points on the distorted curved line (Chang, *et al*, 2017).

By measuring H_m (the crossing point of the two pattern edges) and the slope of edges of the Hough pattern (dotted lines in Figure 10) at H_m, the coordinates of points P_{d1} and P_{d2} in image space can be estimated. H_0, which is the minimum of the smile in Hough space, gives the location where the curve crosses the y axis in image space. By assuming that these three points without distortion are collinear, the distortion parameter can be estimated, as detailed in (Chang et al, 2017). However, this method has several limitations. First, points H_m and H_0 can be difficult to locate accurately in the Hough space. The number of votes received by H_m is very low compared with the upper edge of the Hough pattern. When the image contains multiple segments, the Hough patterns associated with the lines can overlap making it difficult to locate point H_m. Secondly, the low number of votes limits the accuracy with which H_m and the slopes may be extracted, limiting the accuracy in locating the curve end points. Similarly, the y value of the pixel associated with the H_0 can only be measured to the nearest pixel. Finally, only three points may not be sufficient to recover the undistorted line accurately, especially if the accuracy of these three points is limited.

3.3.2. 'Smile' Based Method

An alternative approach is to use the 'smile' to recover the curved line in image space and use the whole of this curve to estimate the distortion parameter and correct the lens distortion. By fitting a smooth curve to all the points on the 'smile', the slope can be estimated, enabling the curved line in image space to be reconstructed. Then by assuming that without distortion the points on the curve are collinear, the lens distortion parameter can be estimated. We name this method 'smile' based lens distortion correction (SLDC). In the next chapter the basic steps of this correction method will be described in more detail.

Inherently, SLDC is more accurate than the feature point based method for three main reasons. First, the 'smile' receives many votes, making it easier to detect and locate. Second, by fitting a smooth curve to the smile, the effects of quantisation and noise can be significantly reduced. It also enables the slope to be calculated more accurately. Finally, by using a larger number of curve points to estimate the lens distortion parameter, the effects of noise (including quantisation) can be further reduced.

By influencing the shape of the Hough pattern, the four features mentioned in the last section affect the accuracy of the correction method. In chapter 5, the influence of these features on the accuracy will be analysed and the worst case where the correction method is still effective will be discussed.

Chapter 4 Smile Based Lens Distortion Correction

Based on the analysis in Chapter 3, a lens distortion correction method was designed. The main steps of this method are shown in Figure 13.
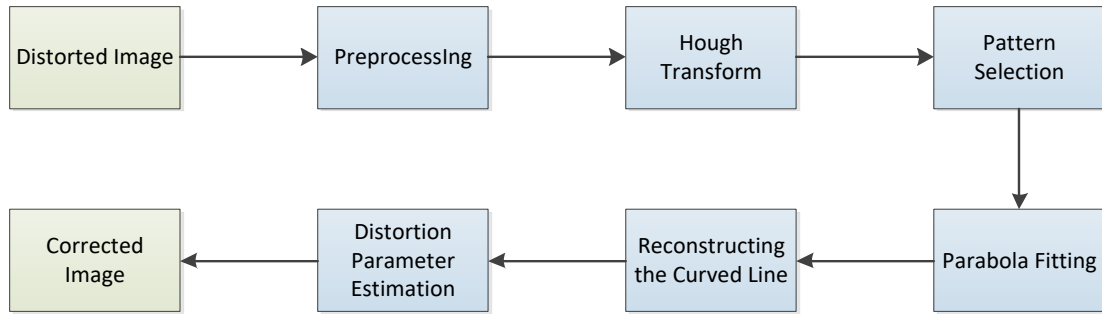
Figure 13: Basic steps of the 'smile' based method

4.1. Preprocessing

The aim of the preprocessing steps is to prepare a suitable input for the Hough transform. The input for the Hough transform should be a binary image which contains edge features only. Therefore, if the input is a colour image it needs to be converted into grey scale. A Canny edge detection filter is applied to the distorted image in order to extract the most significant line segments and arcs in the scene. To suit the original Hough transform, the edges should be detected for the horizontal and vertical directions separately.

Figure 14: The original image (left) and the input for the Hough transform (horizontal and vertical).

4.2. Hough Transform

In this step, the detected edges are transformed into the Hough space. Unlike the standard Hough transform, the original Hough transform needs two mapping for horizontal and vertical directions separately,

$$c_1 = -m_1 x_i + y_i \quad (-1 \leq m_1 \leq 1)$$
$$c_2 = -m_2 y_i + x_i \quad (-1 \leq m_2 \leq 1)$$

(29)

A gradient based Hough transform is used. Most of the lines in manmade scenes tend to be either horizontal or vertical. By limiting the slopes which were measured the gradient Hough transform can reduce computation cost and also reduce the clutter within Hough space making it easier to detect the Hough pattern.

4.3. Selecting the Hough Pattern for Analysis

For real world images, after edge detection there will be not only one edge within the image, thus there will be several patterns in the Hough space. Therefore, selecting the best pattern for analysis becomes an issue. The aim of this selection is to find the Hough pattern corresponding to the most distorted line which would tend to give the most accurate results. We select the Hough patterns by giving them scores. There are two factors have been taken into account that is the length of the line segment (L); the distance from the line segment to the centre (y_0). The L is measured by adding the number of votes within the pattern from the intercept column which contains the maximum vote. The y_0 is measure by the intercept of the Hough pattern. From the results of Chapter 3, a good pattern should correspond to the edge which have large y_0 and L.

Figure 15 (a) and (b) show two examples of the Hough pattern and the scores, a higher score means the corresponding pattern is more suitable to be chosen as the reference to correction distortion.

(a)

(b)
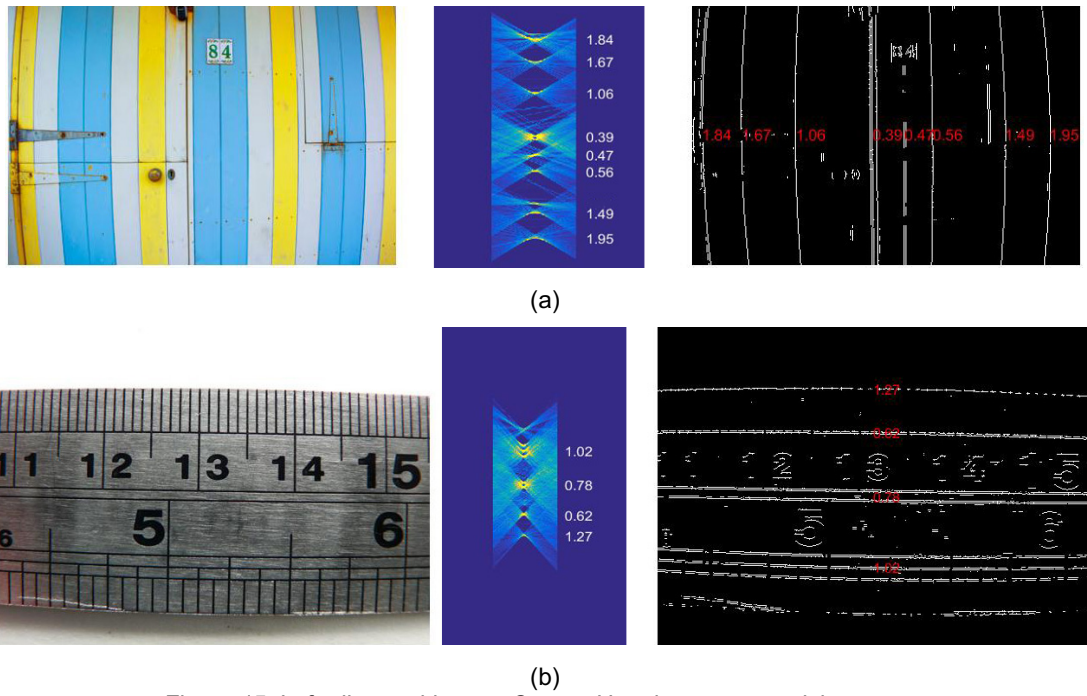
Figure 15: Left: distorted image; Centre: Hough patterns and the scores
Right: detected edges and the scores

Another issue when selecting the Hough pattern is if the edges are too close to each other, their corresponding patterns will be overlapped. An overlapped Hough pattern will bring noise when detecting significant points (picking up points from the other 'smile'). Therefore, when the

pattern is overlapped by another, it will be excluded as a good reference. This is measured by counting the number of votes, if the votes received for measuring the length of the line is over the size of image, we assume that the corresponding pattern is overlapped by another.

Once the pattern is selected, the most significant point (with the maximum votes) for each slope needs to be detected. We collect both the 'm' (slope) and 'c' (intercept) of each significant point for the next step.

4.4. Parabola Fitting

To measure the slope of the 'smile', the data extracted needs to be smoothed. We choose to fit a parabola to the data because the shape of the 'smile' is similar to a parabola (see Figure 16). The general expression for a parabola is:

$$c = P_1 m^2 + P_2 m + P_3 \tag{30}$$

Where P_1, P_2 and P_3 are determined by minimising the squared residuals. The squared error is:

$$E^2 = \sum_i (P_1 m_i^2 + P_2 m_i + P_3 - c_i)^2 \tag{31}$$

Where (m_i, c_i) are the coordinates of a point on the 'smile'. To minimise E^2 in (31) we take the partial derivatives with respect to P_1, P_2 and P_3, and equate these to 0. This gives:

$$\begin{bmatrix} \sum_i m_i^4 & \sum_i m_i^3 & \sum_i m_i^2 \\ \sum_i m_i^3 & \sum_i m_i^2 & \sum_i m_i^1 \\ \sum_i m_i^2 & \sum_i m_i & 1 \end{bmatrix} \times \begin{bmatrix} P_1 \\ P_2 \\ P_3 \end{bmatrix} = \begin{bmatrix} \sum_i c_i m_i^2 \\ \sum_i c_i m_i \\ \sum_i c_i \end{bmatrix} \tag{32}$$

By solving the matrix equation we can determine the parameters of the parabola.

$$P = M^{-1}C \tag{33}$$

These three parameters define the parabola that best fits the significant points. Figure 16 shows the most significant points and the parabola. It is clear that a parabola provides a reasonable fit to the significant points. A detailed analysis of the accuracy of fitting will be discussed in the next chapter.
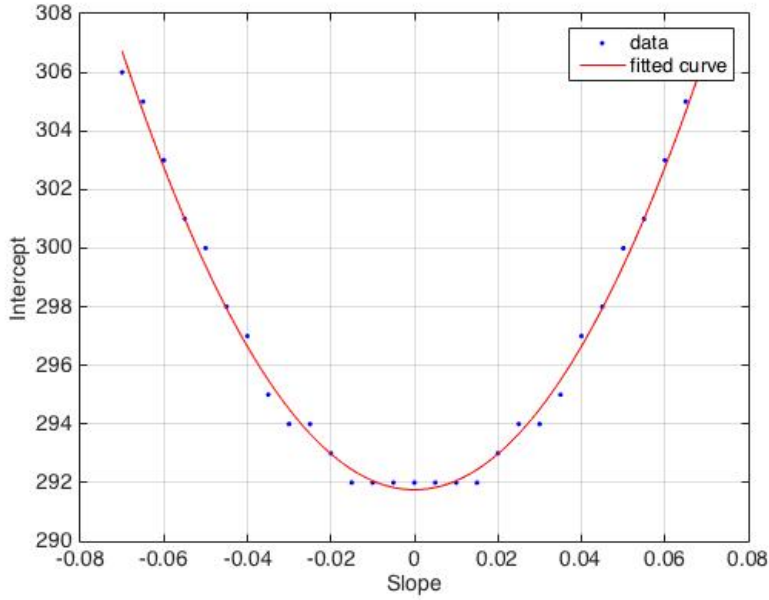
Figure 16: The most significant points and the fitted parabola

4.5. Curved line Reconstruction

As described in the last chapter, the coordinates of a point in the image domain can be calculated from a point on the 'smile' and its slope. From equation (30), the x coordinate in image space is given from the slope of the 'smile':

$$x_i = -slope = -2P_1 m_i - P_2.$$ (34)

The corresponding y coordinate is:

$$y_i = c_i + m_i \times x_i = P_1 m_i^2 + P_2 m_i + P_3 - 2P_1 m_i^2 - P_2 m_i = P_3 - P_1 m_i^2.$$ (35)

Substituting (34) into (35) and eliminating m_i gives a parabola in image space:

$$y_i = P_3 - \frac{(x_i + P_2)^2}{2P_1}.$$ (36)
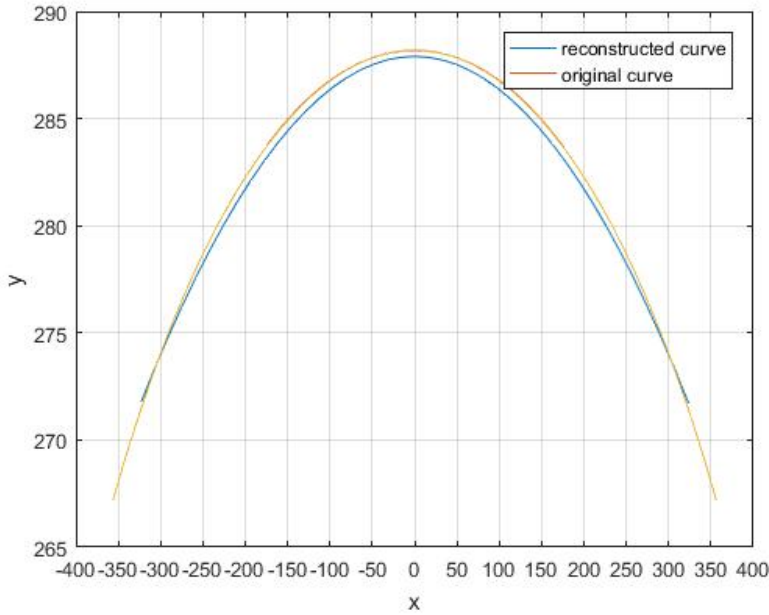
Figure 17: The reconstructed curved line and the original curved line.

In Figure 17 the red arc is the original curved line and the blue arc is the reconstructed curve. The RMS error between the reconstructed curved line and the original curved line is less than 1 pixel and a detailed analysis will be presented in the next chapter.

4.6. Estimating the Lens Distortion Parameter

The reconstructed curved line should be straight without distortion. By mapping points on the reconstructed curved line by an inverse distortion model and measuring the straightness of the mapped points the distortion parameter can be estimated.

From the approximate inverse distortion model (10), we have:

$$r_u = r_d - r_d \left(\frac{\kappa r_d^2 + \kappa^2 r_d^4}{1 + 4\kappa r_d^2} \right) \tag{37}$$

the x and y coordinate of the point on the undistorted straight line can be represented as:

$$\begin{cases} x_u = x_d \left(1 - \left(\frac{\kappa r_d^2 + \kappa^2 r_d^4}{1 + 4\kappa r_d^2} \right) \right) \\ y_u = y_d \left(1 - \left(\frac{\kappa r_d^2 + \kappa^2 r_d^4}{1 + 4\kappa r_d^2} \right) \right) \end{cases} \tag{38}$$

From (38) y_d can be represented as a function of x_d, if we assume the equation of the original straight line is $y = Ax + B$, Then the distance from (x_u, y_u) to the original straight line can be represented as:

$$D = \frac{|Ax_u - y_u + B|}{\sqrt{1 + A^2}}$$

(39)

For all the point the least squares equation can be written as:

$$S = \sum_i \frac{(Ax_u - y_u + B)^2}{1 + A^2}$$

(40)

Since we have the equation of the parabola, (40) can be represented continuously as:

$$S = \int_{x_{d1}}^{x_{d2}} \frac{(Ax_u - y_u + B)^2}{1 + A^2} dx_d$$

(41)

where x_{d1} and x_{d2} are the x coordinates of the endpoints of the reconstructed curved line. When substituting (38) into (41) there are three unknowns, namely A, B and κ. When the original line segment is horizontal or vertical, 'A' can be set to 0. To minimise S in (41) we take the partial derivatives with respect to A, B and κ and equate these to 0. By solving the resulting set of equations numerically the lens distortion parameter can be estimated. Once the distortion parameter is estimated, the lens distortion can be corrected by reverse mapping based on the distortion model.

Chapter 5 Accuracy Analysis

5.0. Overview of the Accuracy Analysis
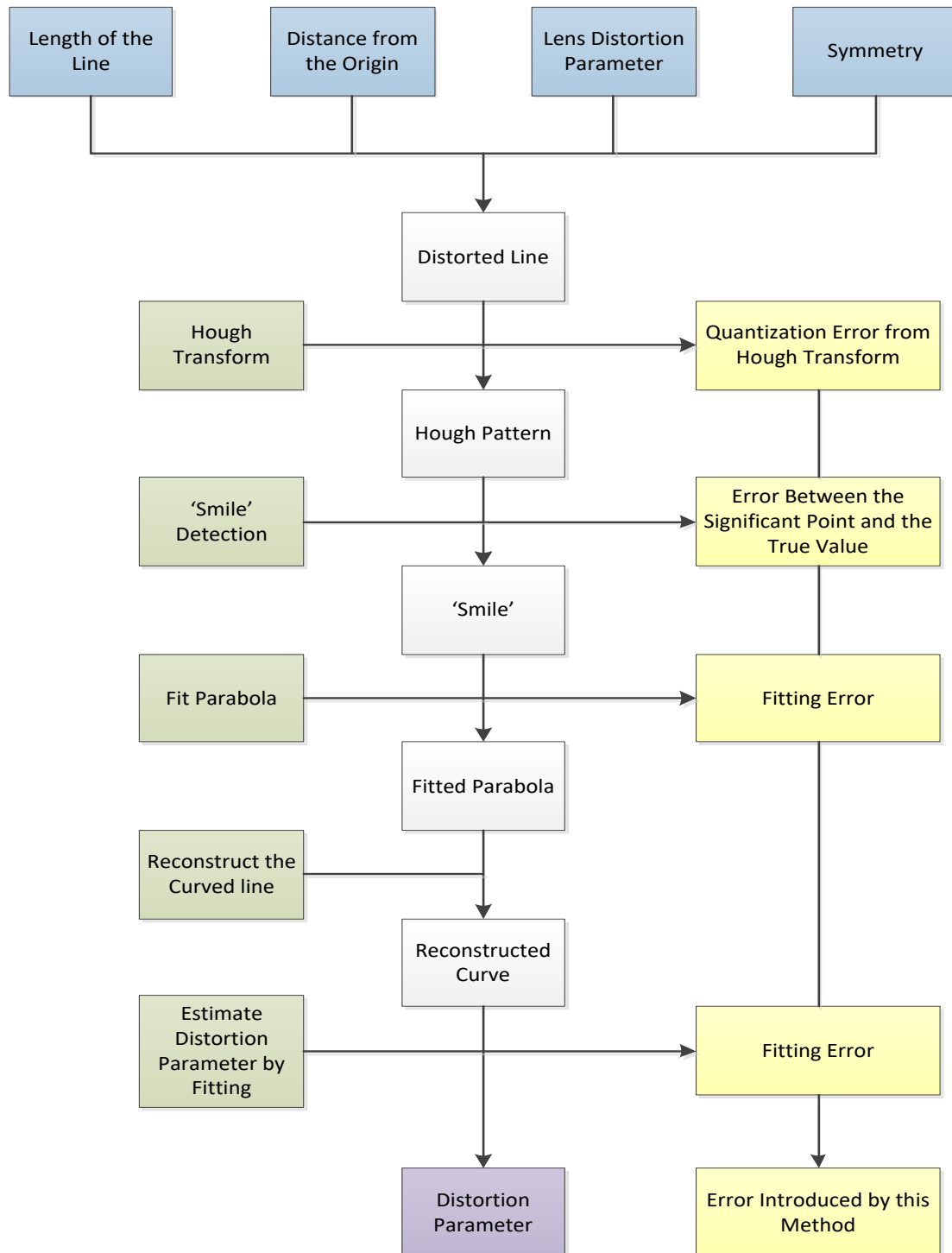
Figure 18: Basic Steps of the 'Smile' based method and the errors introduced by this method

Figure 18 identifies the basic steps of the SLDC and the error introduced by each step. The four blue blocks in the first row represent features of the original line segment. As identified in Chapter 3 these four factors have a strong influence on the features of the 'smile', and therefore have a significant influence on accuracy. By analysing these four factors the worst case where the SLDC still valid can be investigated.

The grey blocks in the centre column represent how the information of the distorted line is transformed in this method. The transformation starts with a curved line and ends with the reconstructed curved line which is used to estimate the distortion parameter. In ideal cases (without quantisation and noise), this reconstruction should introduce no error, the reconstructed line should be the same as the original one.

The light green blocks (left) in the right column represent the basic steps involved in this correction method. After each step the information of the curved line will be transformed into a different form. However, because of quantisation, noise and modelling error, some steps introduce error. The error introduced by each step is indicated by the yellow blocks (right column). Combining the errors together gives the overall error introduced by the SLDC.

In this chapter, an accuracy analysis is applied to the SLDC. Both ideal and general cases will be covered. The aim of this analysis is to identify the systematic and random error introduced by the SLDC, and investigate the worst cases where it is still valid. Factors which influence the accuracy of this method will be discussed. Attempts to increase the accuracy will be presented. This analysis starts with identifying the relation between the error in the estimated lens distortion parameter and the position error of pixels within the image.

5.1. Error in the estimated lens distortion parameter and the RMSE of the image

The 'smile' based lens distortion correction method works by estimating the lens distortion parameter (κ). However, the error in κ cannot represent the position error of pixels directly. One metric of the position error is the root-mean-square error (RMSE) between each pixel in the corrected image with its undistorted position. When there is no error in the estimated lens distortion parameter, the RMSE should only result from the approximation of distortion model. In the simulation, the original line segment is distorted with a given distortion parameter. When correcting we add an error to the distortion parameter (κ_e). Figure 19, 20 and 21 show the relationship between the error in lens distortion parameter (κ) and the RMSE of the corrected line segment. We analyse this combination with the factors which influence the shape of the line segment (κ, L and y_0). The radius of the corrected point is represented as (42),

$$r_u \approx r_d - r_d \left(\frac{(\kappa + \kappa_e)r_d^2 + (\kappa + \kappa_e)^2 r_d^4}{1 + 4(\kappa + \kappa_e)r_d^2} \right) \tag{42}$$

the r_d is equal to $\left(\frac{L^2}{4} + y_0^2\right)^{\frac{1}{2}}$, the error in κ is κ_e. This analysis is based on an 800×800 image, with the centre of this distortion is in the centre of the image. The line segment within the image is symmetric about the distortion centre. All quantities are normalised, such that the radius of the image is 1 (i.e. $r = 1$ corresponds to 400 pixels).

Figure 19 shows the relation between the RMSE and the error in the estimated κ with a changing distortion parameter. The RMSE increases with the increase of the error in κ. When the distortion is serious, same error in the estimated κ results with a higher RMSE. When the error in estimated κ is less than 2.5×10^{-3}, the RMSE is less than 1 pixel.
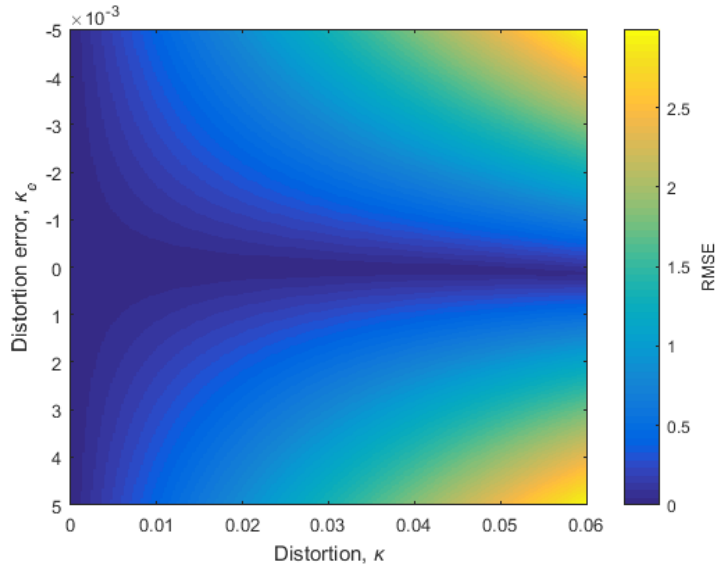
Figure 19: RMSE with varying κ and error in the estimated κ, when $L = 1$ and $y_0 = 1$.
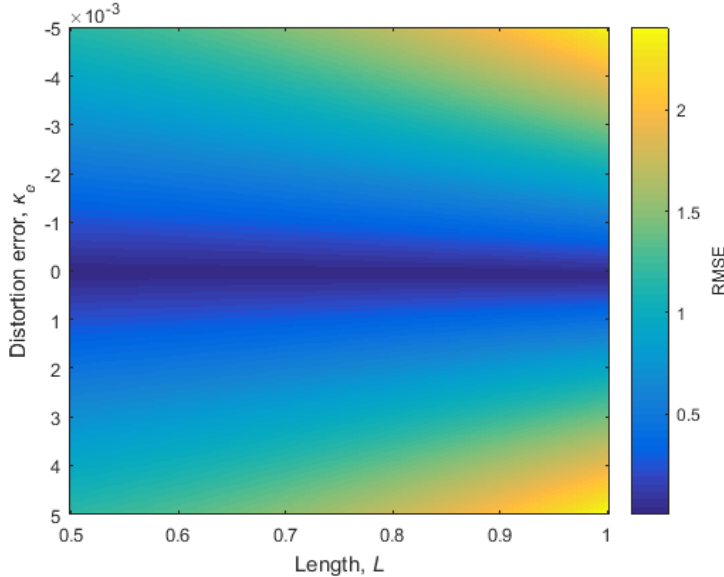
Figure 20: RMSE with varying L and error in the estimated κ, when $\kappa = 0.05$ and $y_0 = 1$.

In Figure 20 shows the effects of the length of the line segment (L) on error. The RMSE increases with the increase of the length of the line segment. This is because points further

from the centre suffer from more distortion. Therefore, error in estimating the distortion parameter will have more effect near the edge of the image. A longer line segment has more points which are near the edge of the image and these will result in a larger RMSE even with the same error in κ.
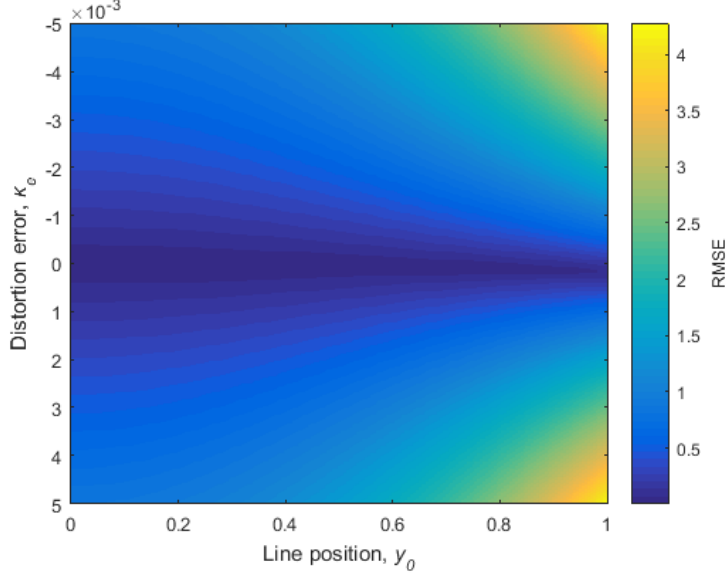
Figure 21: RMSE with varying y_0 and error in the estimated κ, when $\kappa = 0.05$ and $L = 1$.

Figure 21 shows the relation between the effect of line segment position relative to the centre of the image (y_0). The RMSE is higher when y_0 is larger, because the line is near to the edge of the image.

In Figure 19, 20 and 21, when the error in estimated lens distortion parameter is less than 2.5×10^{-3} the RMSE is less than 1 pixels. Figure 22 compares a real-world image before distortion and the corrected image with a 2.5×10^{-3} error in the distortion parameter. The difference is hard to identify through human vision. So, in this research we assume an error less than 2.5×10^{-3} in the estimated lens distortion parameter is acceptable.

Figure 22: Left: The undistorted image; Right: the corrected image with 2.5×10^{-3} error in κ.

5.2. Error when Using Continuous Data to Correct Distortion
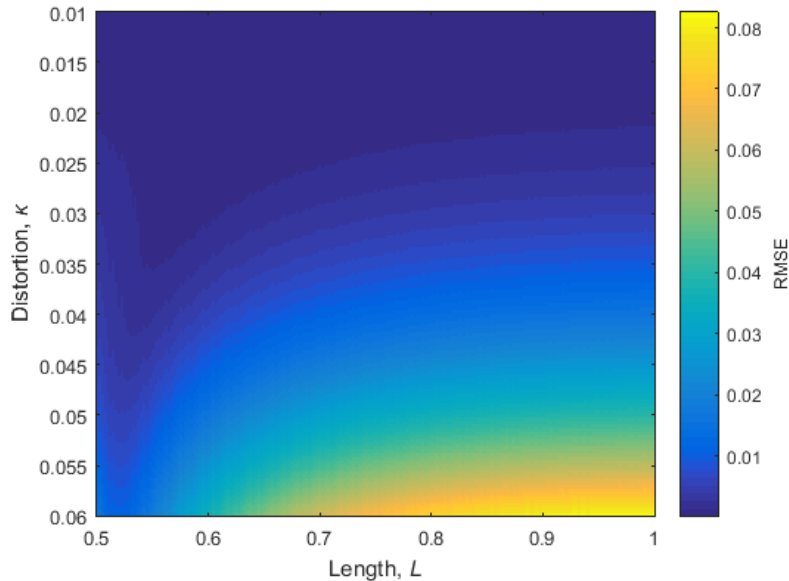
As shown in Figure 18, one of the key contributions to the error in this correction method comes from quantisation. To demonstrate the accuracy what this method can achieve without quantisation, a simulation with continuous data was performed. The accuracy was measured by the RMSE between the corrected line segment and the undistorted line segment (ground truth). For simplicity, we assume the centre of the image is the centre of the distortion, and the line segment is symmetric about the distortion centre. This simulation starts with a line segment $y = y_0$, then it is distorted by a given lens distortion parameter. Instead of detecting the 'smile' in the Hough transform space, it was calculated analytically from the tangential line through a point on the distorted curve. Therefore, there will be no influence from quantisation in this simulation. The smile was given by the following equations:

$$m_i = slope = -\frac{2\kappa y_0 x_{ui}}{3\kappa x_{ui}^2 + \kappa y_0^2 + 1}$$
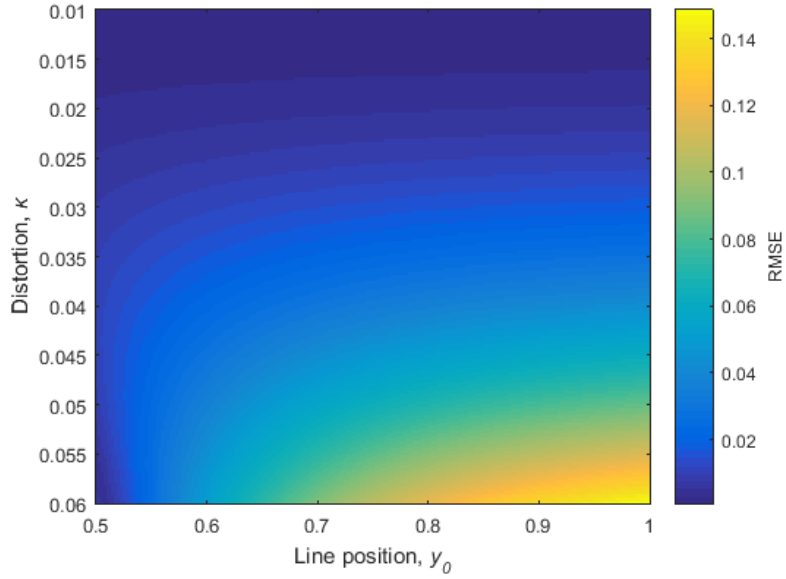
$$c_i = intercept = y_0 + m_i x_{ui}$$

(43)

Where (x_{ui}, y_0) are the coordinates of a point on the undistorted line segment and (m_i, c_i) are the coordinates of a point on the 'smile' in the Hough transform space.
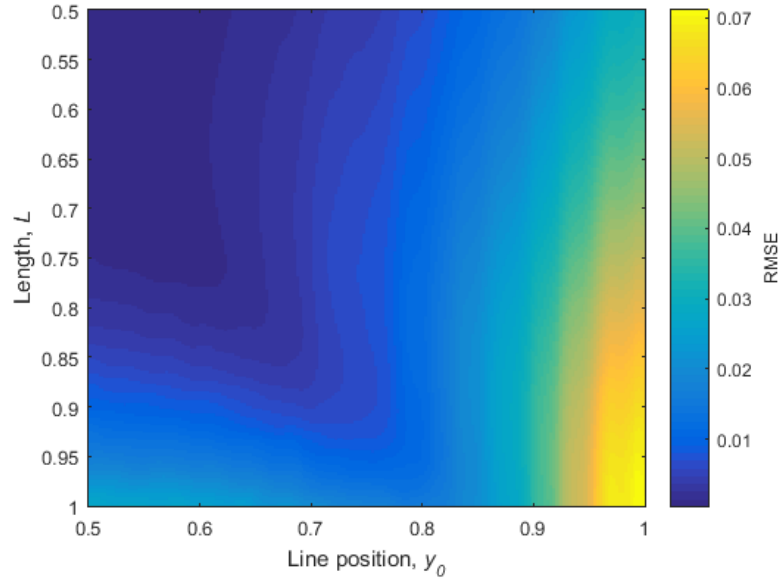
Three factors (κ, L and y_0) which influence the shape of the original distorted line are taken into account in this simulation. The influences on accuracy of these three factors are shown in Figure 23. In all three plots, the error is higher where the distortion is more significant, it is the result of the approximation reverse model. However, the highest error is less than 0.14 pixels which is insignificant.

(a) the RMSE with varying κ and L ($y_0 = 1$).

(b) the RMSE with varying κ and y_0 ($L = 1$).

(c) the RMSE with varying L and y_0 (κ=0.05).

Figure 23: Different parameters and the accuracy of the estimated lens distortion parameter.

5.3. Systematic and Random Error of the SLDC

In this section, the systematic error and the random error of the 'smile' based method will be investigated. From the previous analysis, when the data is continuous and without quantisation the RMSE of this method is less than 0.15 pixels, this error can then be neglected for most applications. However, the Hough transform data is quantised by the voting process, which introduces error into the measurement. The accuracy when fitting a parabola to the 'smile' is

also essential to the error introduced by this method. Other aspects which will bring error to the SLDC will also be discussed in this section.

5.3.1. The 'Smile' and the True Value

As analysed in Chapter 3, a point on the curved line and its tangent in image space correspond to a point in Hough transform space, located at the curved edge of the Hough pattern. Therefore, the edge of the Hough pattern corresponds to the 'true value' of the curved line. However, we detect the 'smile' from the most significant point (most votes) for each slope. The most significant point is offset from the edge of the Hough pattern by the voting process.

In the Hough transform space, for each slope ('m' value) the received votes changes with the intercept ('c' value). When the intercept is closer to the curved edge of the Hough pattern the votes became higher, see Figure 24 (right). If the data is continuous the votes can be represented by their density.
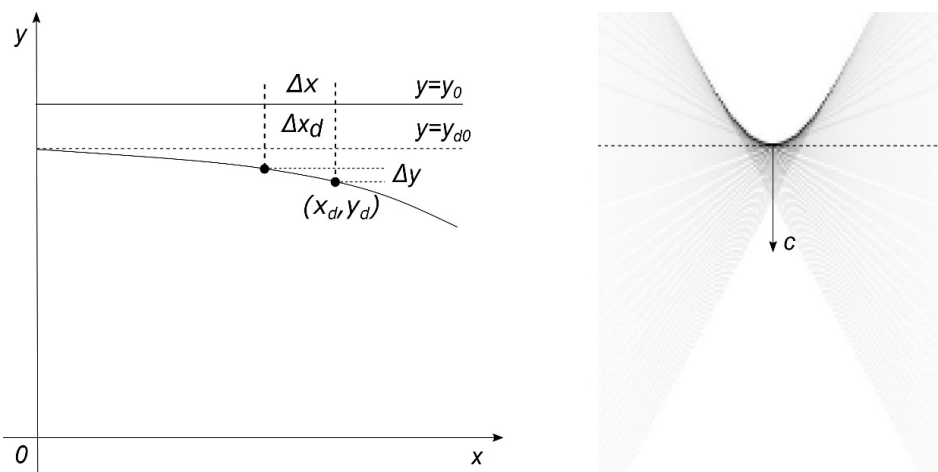
Figure 24: Δc and Δx in the image space for $m = 0$.

Take the case where the original line segment in image is horizontal as an example, in Figure 24 it is represented as $y = y_0$. The dotted line $y = y_{d0}$ corresponds to the minimum point of the upper edge of the Hough pattern when $m = 0$. Here, we define the horizontal axis of the density plot, c_d, as the distance from a point to the upper edge, see in Figure 24 (right). And that distance is equal to the vertical distance between the dotted line y_{d_0} to a point on the curve y_d. We assume the coordinate of a point on that curve is (x_d, y_d). So c_d can be represented as:

$$c_d = y_{d_0} - y_d \tag{44}$$

From the lens distortion model we have:

$$\begin{cases} y_d = y_0(1 - \kappa(x^2 + y_0^2)) \\ x_d = x(1 - \kappa(x^2 + y_0^2)) \end{cases} \tag{45}$$

where the x is the parameter of the original straight line. When the line is horizontal the density can be represented as:

$$density = \frac{\Delta x_d}{\Delta y} = \frac{(x + \Delta x)\left(1 - \kappa\left(((x + \Delta x)^2) + y_0^2\right)\right) - x(1 - \kappa(x^2 + y_0^2))}{\left(y_{d_0} - y_0\left(1 - \kappa((x + \Delta_x)^2 + y_0^2)\right)\right) - \left(y_{d_0} - y_0\left(1 - \kappa(x^2 + y_0^2)\right)\right)} \qquad (46)$$

After simplifying and ignoring the high order components of Δx, we have:

$$density \approx \frac{1 - 3\kappa x^2 - \kappa y_0^2}{2\kappa y_0 x} \qquad (47)$$

From equation (44):

$$c_d = y_0 - y_d = y_0(1 - \kappa y_0^2) - y_0(1 - (x^2 + y_0^2)) = y_0 \kappa x^2 \qquad (48)$$

Rearranging to get x gives:

$$x = \sqrt{\frac{c_d}{\kappa y_0}} \qquad (49)$$

Now the density can be represented as:

$$density = \frac{1 - 3y_0^{-\frac{1}{2}}(\kappa c_d)^{\frac{1}{2}} - \kappa y_0^2}{2(\kappa y_0)^{\frac{1}{2}} c^{\frac{1}{2}}}$$

$$= \frac{1}{2(\kappa y_0)^{\frac{1}{2}} c_d^{\frac{1}{2}}} - \frac{3c^{\frac{1}{2}}}{2\kappa^{\frac{1}{2}} y_0^{\frac{3}{2}}} - \frac{(\kappa y_0)^{\frac{1}{2}}}{c_d^{\frac{1}{2}}} \qquad (50)$$

Figure 25 shows the density plot based on equation (47). It is clear that the highest density is close to the upper edge of the Hough pattern.

When the original segment is not horizontal, the vote density has a similar result. However, because of quantisation in the Hough transform space, the most significant points may not be located at the edge of the Hough pattern. If we define the 'smile' by the most significant points, it may not relate to the true value of the curve in the image space. The influence of quantisation will be discussed in the following section.
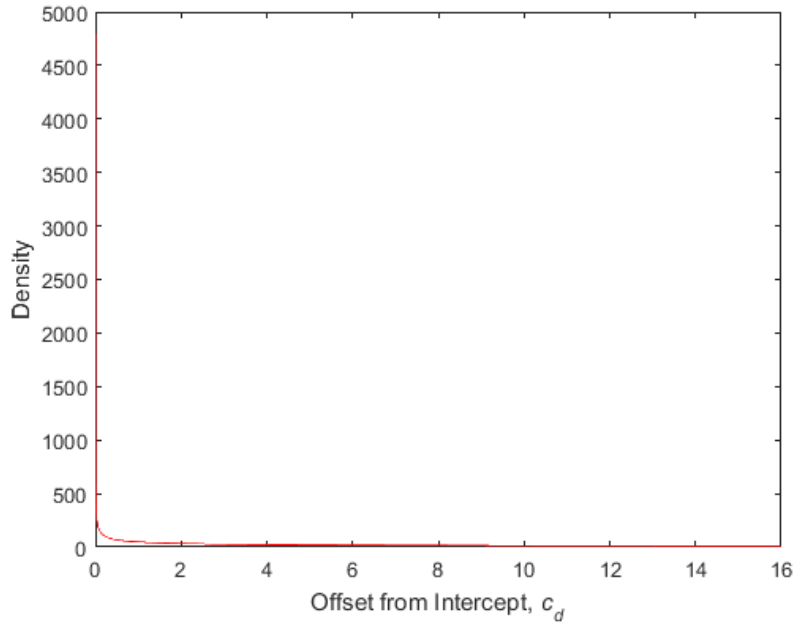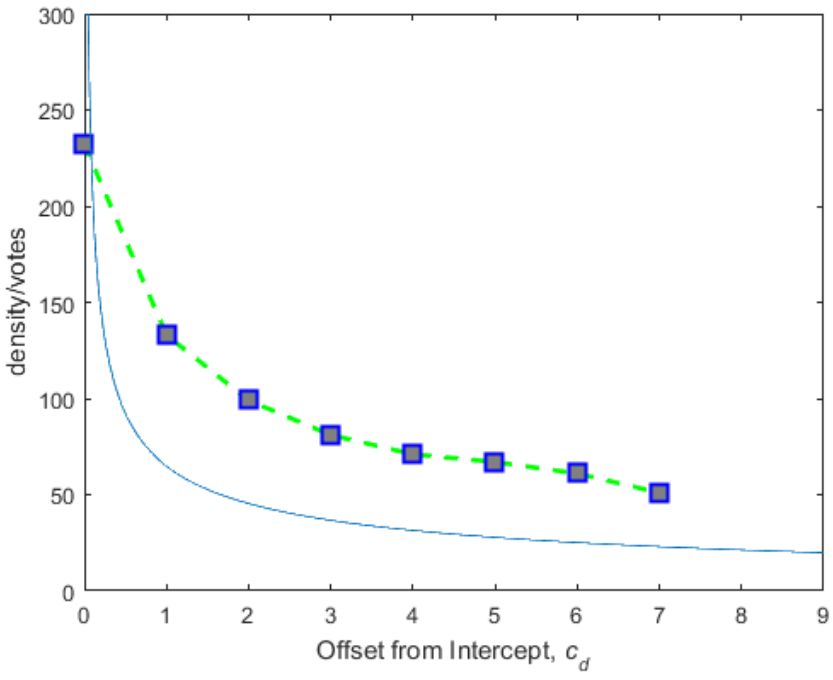
Figure 25: Relation between density and intercept.

5.3.2. Error from Quantisation
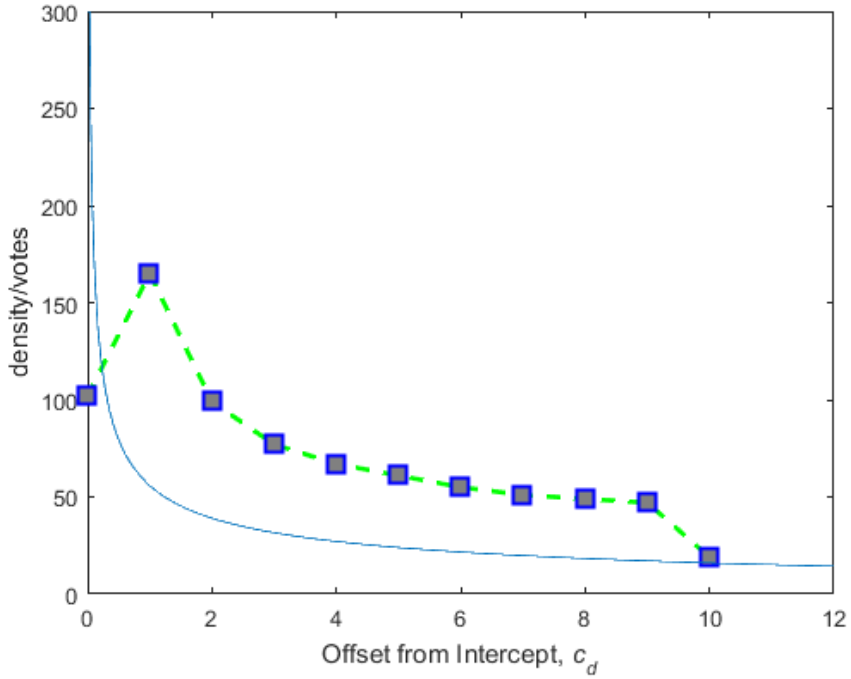
The last section analysed the density of votes based on continuous data. However, neither the image domain nor the Hough domain are continuous in this application. The pixel is the smallest addressable element in the image domain, and the Hough domain is quantised into bins. The coordinates of each bin in the original Hough domain are addressed by the slope and intercept.

From the density analysis, when the data is continuous the edge of the Hough pattern (true value) is very close to the highest density. However, in the Hough domain the intercept values are quantised into integers. Therefore, the intercept with the highest votes only approximate the position of the highest density. The distance between the highest vote and the highest density is less than one pixel, because the intercept is quantized into an integer, usually of the resolution of one pixel in the image domain. Figure 26 shows two possible situations of the highest vote and density.

In Figure 26 (a) and (b) the blue line is the plot of the continuous density, and the dots represent votes in Hough domain. The zero offset of the 'c' value is the edge of the Hough pattern. In Figure 26 (a) the edge of the Hough pattern received the highest votes, in Figure 26 (b) the highest vote is located at the second intercept bin. However, for both situations the distance from the highest vote to the highest density is less than one pixel. Although we can control the resolution of the Hough space, there will still be influences from quantisation.

42

(a)

(b)

Figure 26: The effect of quantisation on the density of votes for two different values of the lens distortion parameter.

When the line segment is not horizontal, the relation between the intercept bin of highest vote and density is the same. The difference between the intercept bin of the highest vote and the intercept bin of the highest density is less than one pixel. So, in the Hough domain, defining the

'smile' by the set of points with the highest vote, the detected 'smile' will be different from the true value. For each slope value the error of the detected intercept is less than one pixel. Figure 27 shows the detected 'smile' and the true value.
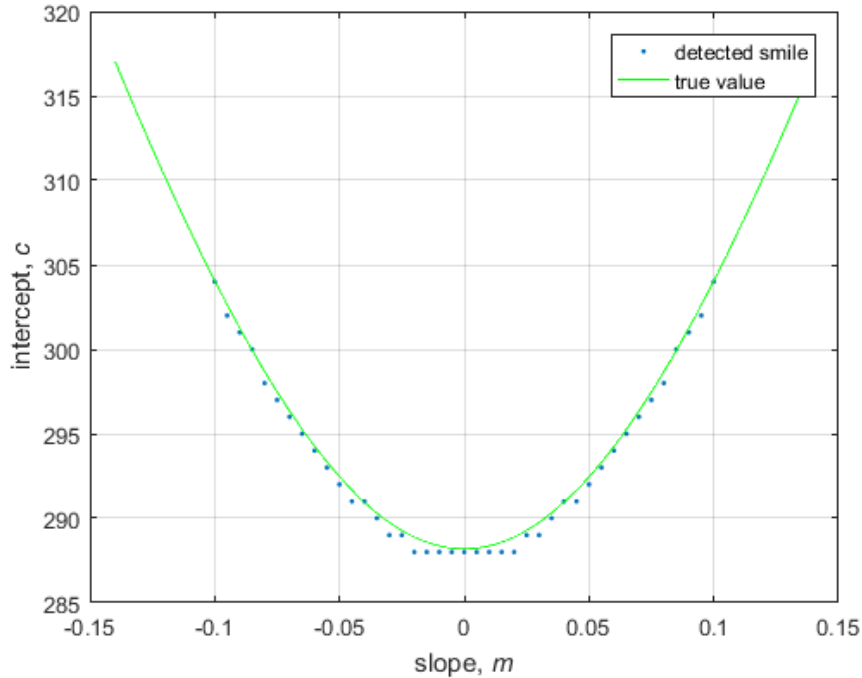
Figure 27: The most significant points and the true value.

In Figure 27, the blue dots are the points with the highest vote for each slope value, and the green curve represents the continuous data. (Note that the detected maxima are biased on one side of the true curve, resulting from the tail of the density curve).

5.3.3. Error from Fitting

To smooth the data collected in the last step, we fit a parabola to the 'smile'. The reason for choosing a parabola is because the shape of the 'smile' is similar to it. Figure 28 compares the significant points and the fitted parabola and the true value. It is clear the fitted parabola (red) is closer to the true value. The fitting can also reduce the error introduced by quantisation noise and make it easier to measure the slope of the 'smile'.

As can be seen in Figure 28, the fitted parabola follows the trace of the true value and the error from the fitted parabola to the true value is **less than one pixel**. However, there is a consistent bias, which is more noticeable in the centre of the smile. As a result, there is also small error in the slope, which is used to determine the points on the distorted line segment in the image.
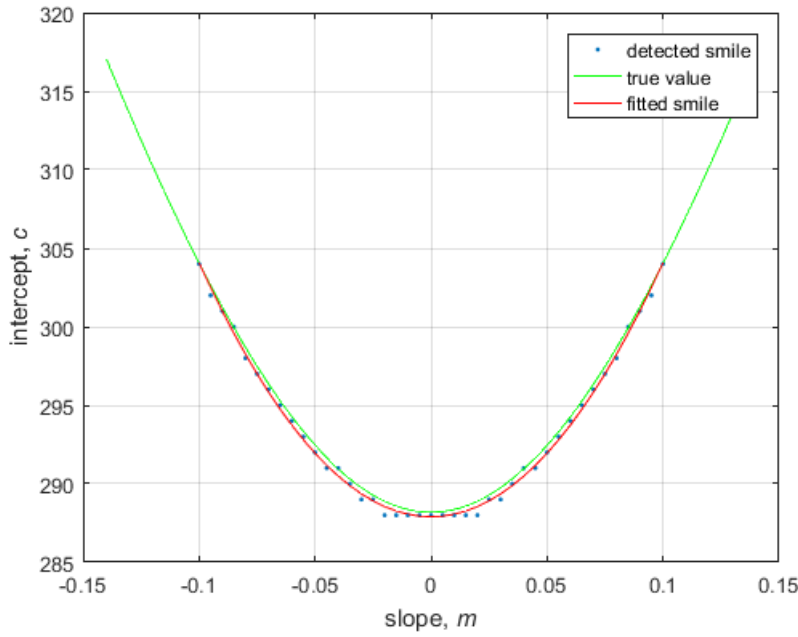
Figure 28: Smoothed detected smile (red) compared to the true smile (blue).

Additionally, we also considered high order polynomial for fitting the 'smile'. Table 1 compares the RSME from fitting a parabola and a 4th order polynomial. The accuracy increases by fitting the data into a high order polynomial is insignificant. Taking the calculation requirement into account in this study we assume a parabola is sufficient to show the trace of the significant points.

Lens distortion parameter	0.041	0.042	0.043	0.044	0.045	0.046	0.047	0.048	0.049
RMSE 2nd order	0.26	0.38	0.30	0.28	0.34	0.29	0.33	0.26	0.33
RMSE 4th order	0.26	0.30	0.29	0.27	0.35	0.27	0.34	0.26	0.29

Table 1: The RMSE of the parabola and the 4th polynomial with different κ.

Another issue is to determine where to stop fitting. From Chapter 3, the 'smile' stops when the edge of Hough pattern become straight. However, it is hard to measure the slope of the 'smile' from quantised data. Instead, we use the number of votes for each slope ('m') to determine where to stop fitting. On the 'smile' the points with higher votes locate near the centre, and the number of votes decreases away from the centre. However, only using the data near the centre cannot provide an accurate fit, because determining the parabola parameters needs more data away from the centre. However, for points which away from the centre, with the decrease of votes, the data is likely to be more affected by noise. To find the threshold to stop fitting, a simulation has been done. In this simulation we use the number of votes of the point on the 'smile' as the reference to define the threshold of stopping the fit. The number of votes is divided by the maximum vote on the 'smile' and compared to a threshold level. A group of data with different distortion levels have been tested, with the result is shown in Figure 29. When the threshold is 0.47 of the maximum vote on the 'smile', the error in the calculated distortion

parameter is the minimum. Therefore, we took 0.47 as the threshold to stop fitting in this method.
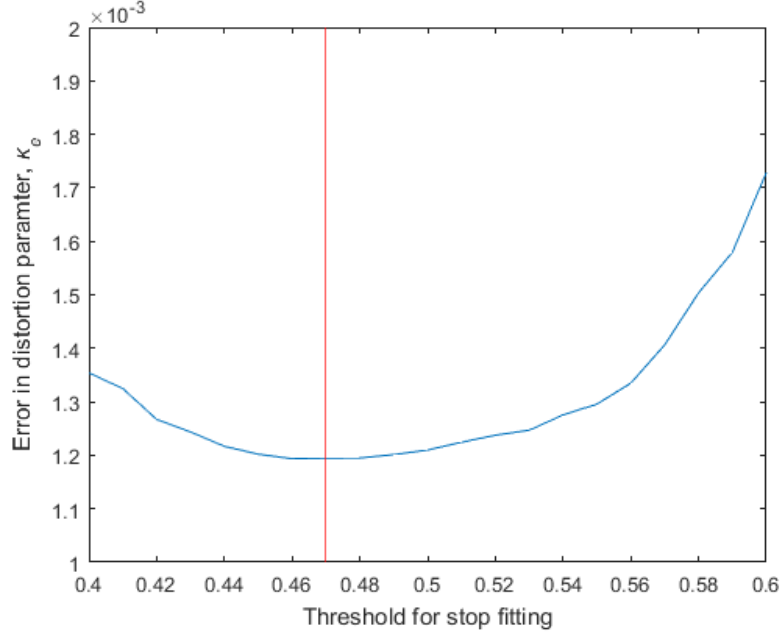
Figure 29: The effect of fitting threshold on estimated lens distortion parameter.

5.3.4. Error in Reconstructing the Curved Line

There is a point to point mapping from the 'smile' parabola to the distorted line and there is no quantization between this mapping. Therefore, the mapping from the parabola to the reconstructed curve will introduce no error. Figure 30 shows the error of the reconstructed curved line relative to the original curved line. The reconstruction error is less than one pixel.
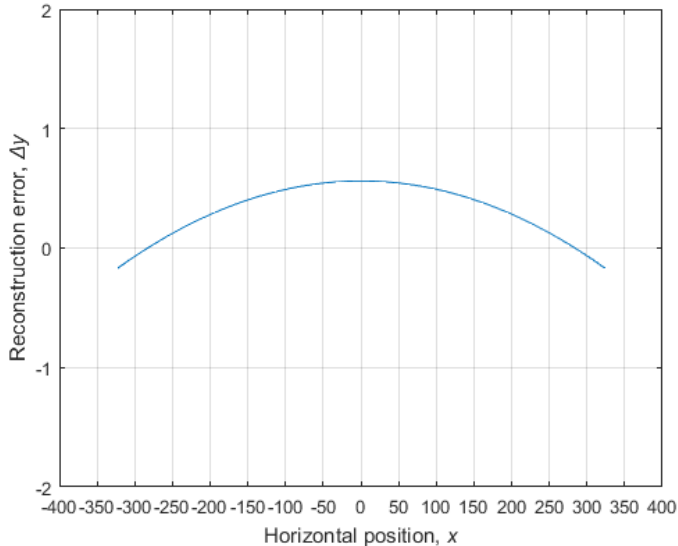
Figure 30: Reconstruction error of the vertical position of the reconstructed line.

5.3.5. Error from Noise

Unlike quantisation, the influence of noise is more random. To investigate the effect of noise on accuracy a simulation has been designed. This simulation tests the influence of noise in the original curved line to the reconstructed curved line. In this simulation the size of the image is 800×800, the length of the line is the length of the image. We added noise to the vertical position of the edge. Figure 31 compares the original curved line without and with noise.
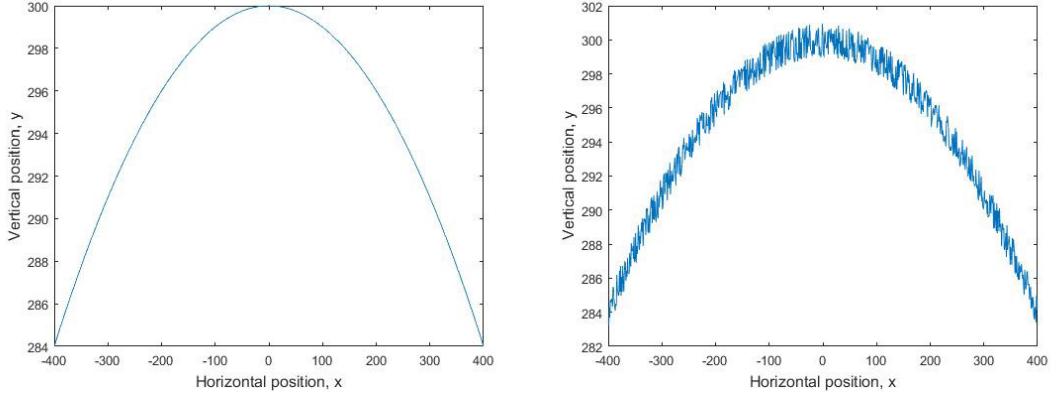
Figure 31: left: the curved line without noise; right: curved line with random noise added.

When detecting the curved edge, we chose to use a Sobel filter, because in Canny edge detection algorithm the edge is smoothed with a Gaussian filter. Then the detected edge is transformed into Hough space and then reconstructed as a curved line. Table 2 shows the RMSE between the original curved line and the reconstructed line; the noise level increase from 0 to 1 pixel in this simulation. The RMSE increases as the noise level increases. However, when the noise is 1 pixel, the RMSE increased only 0.2 pixel which is insignificant. This is because the Hough transform is robust to noise.

Noise	0	0.1	0.2	0.3	0.4	0.5	0.6	0.7	0.8	0.9	1.0
RMSE	0.07	0.08	0.08	0.09	0.12	0.17	0.19	0.21	0.24	0.24	0.28

Table 2: The noise level and the RMSE of the line segment.

5.3.6. Error of the Estimated Lens Distortion Parameter

The lens distortion is estimated by minimising the squared error residuals when fitting the points on the reconstructed curve into a straight line. There are two aspects which bring error in this step, the error introduced by the least square fitting and the error introduced by the approximate reverse lens distortion model. In simulation when correcting an 800×800 image with significant distortion, the absolute error in the estimated distortion parameter is less than 2.5×10^{-3}. The error mainly comes from the quantisation from the bins in parameter space when accumulating the Hough transform. In the following part of this chapter, more general cases will be analysed, and attempts to increase the accuracy will be discussed.

5.4. Accuracy of General Cases

5.4.1. Three Factors of the Line Segment

In this section the factors which influence the shape of the Hough pattern will be analysed and the worst case where this method can still work will be discussed. There are three parameters which influence the shape of the Hough pattern as described in previous sections, that is:

1. The length of the straight line (L).

2. The distance from the straight line to the origin (y_0).

3. The lens distortion parameter (κ).

Since the errors in this correction method are from quantisation and we do not have an expression to represent this error, we chose to use a Monte Carlo simulation to analyse the influence of these three factors. The factors were analysed two by two, and the following plots show the results. In each simulation one factor is fixed and the other two factors are varied. For the Monte Carlo simulation, all three factors are perturbed by a small random amount to reduce local effect from quantisation. The detailed description will be given with each plot. The simulation is applied to an 800×800 image and the parameters of the plot are given as normalized data. The error is measured by RMSE between the corrected line and the given line segment within the image. If the RMSE is higher than 1 pixel then the method is considered to have failed to correct the distortion.
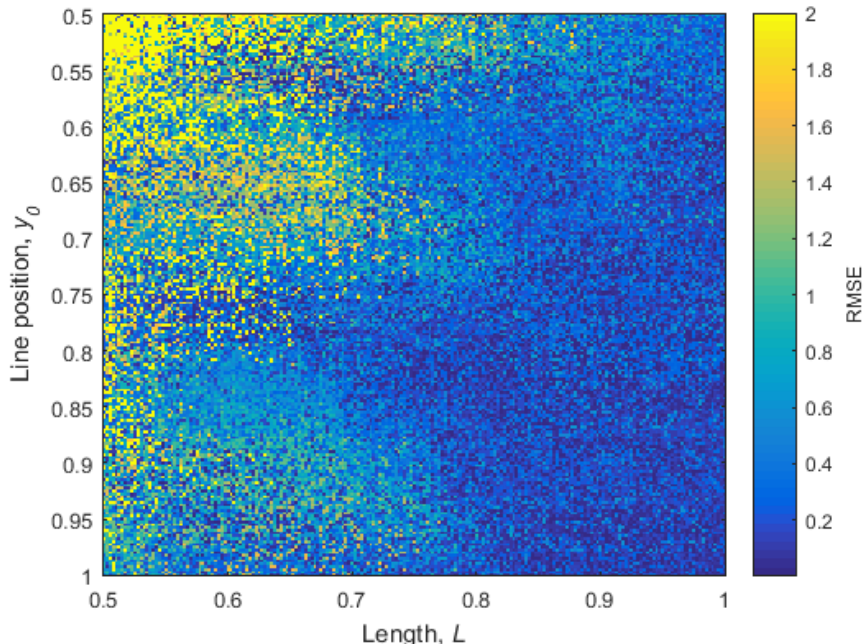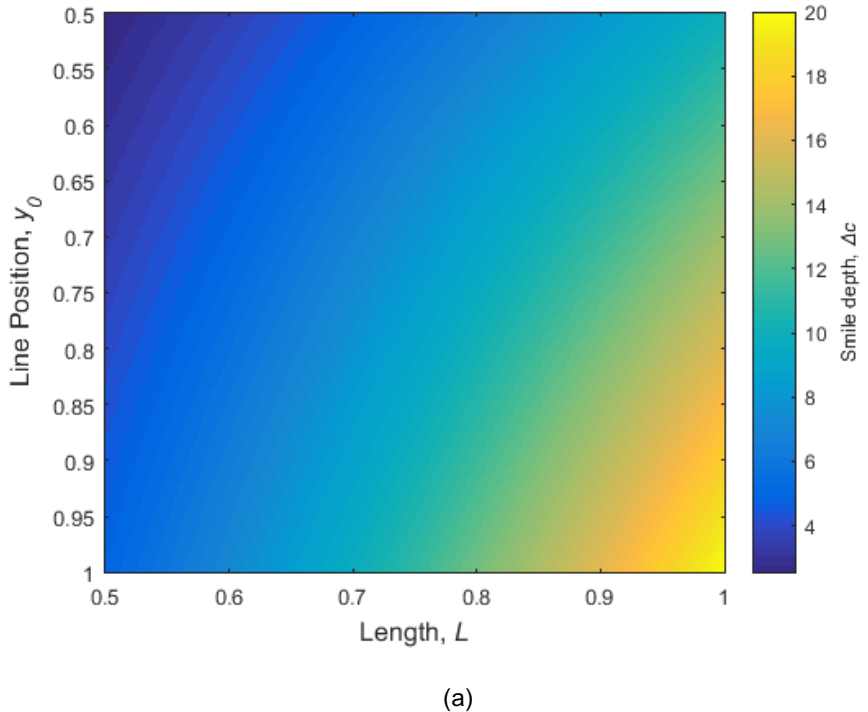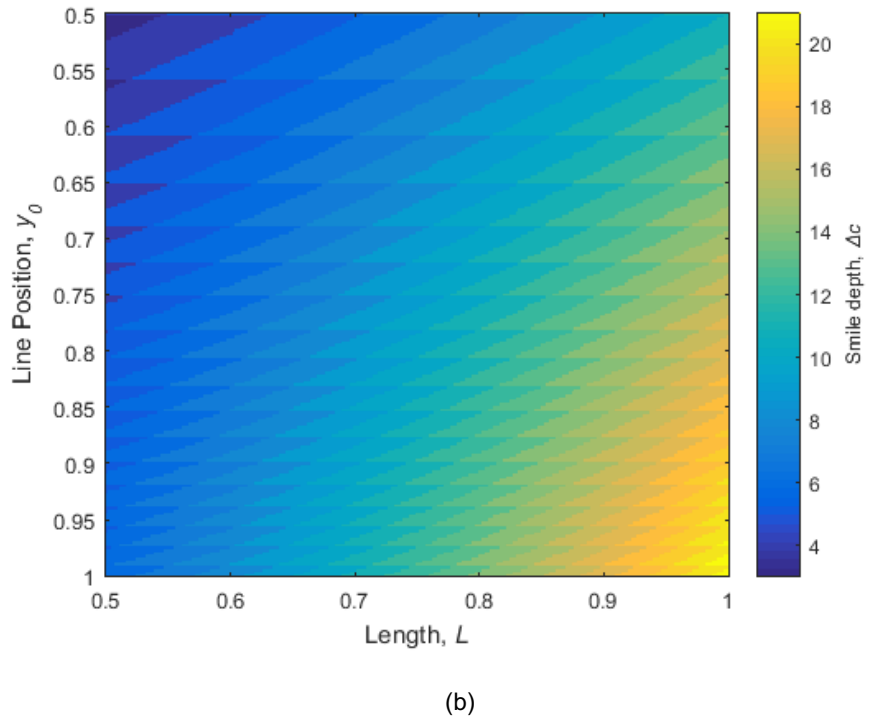
Figure 32: Influence of y_0 and L on error when $\kappa = 0.05$

Figure 32 analyses the influence of L and y_0, in simulation these two factors varied from 0.5 to 1. The distortion parameter in this simulation is 0.05 and with a $\pm 5\%$ random factor. It is clear that when L less than 0.75, the error is more likely higher than 1 pixel especially for smaller values of y_0. This is because when the line is close to the centre and with a short length, it appears with very slight distortion. The Hough pattern is close to a concentrated point which is hard to fit a parabola to. Therefore, for a short curve with sight lens distortion, it is not a valuable reference to correct the distortion.

As can be seen in Figure 32 the RMSE has an underlying pattern. This results from quantisation in Hough transform. Figure 33 compares Δc (the distance between the minimum of the 'smile' to the intersection of the Hough pattern edges) from continuous data and quantised data. With the change of the L and y_0 the size of the Hough pattern changes. It is clear without randomization, the plot of the quantized data appears with a pattern, and it is the reason why the plot of RMSE appear with patterns.

(a)

(b)

Figure 33: (a): delta c from continuous data; (b): delta c from quantized data.

To reduce the influence of quantization and make the plot smooth instead of structured, the L and y_0 are also randomized (± 5 pixels) during the simulation. The change of Δc can be used to represent the change of the shape of Hough pattern, it is clear that when L and y_0 are small, the Hough pattern is more compact, making it difficult to analyse, and results with high errors.
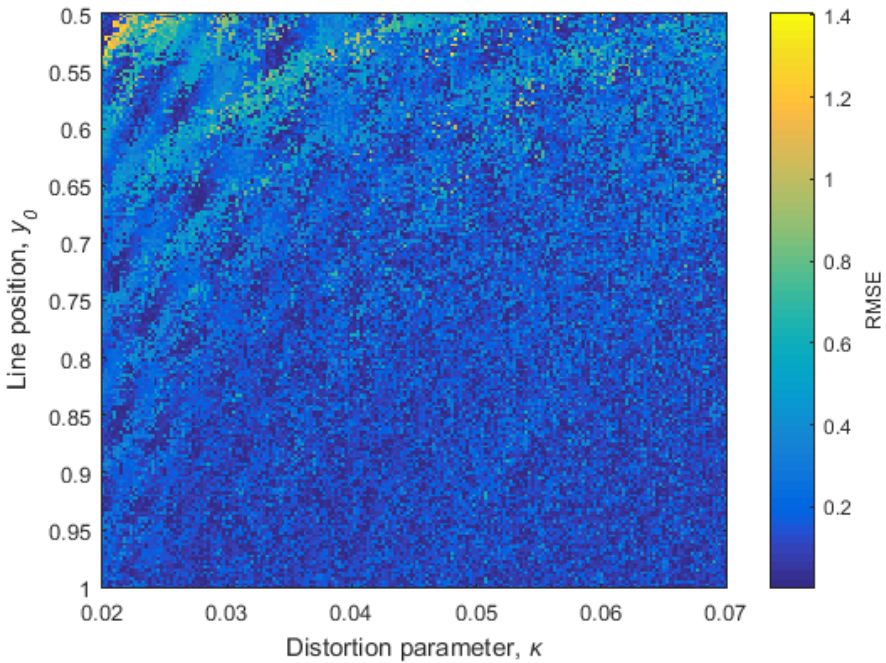
Figure 34: Influence from y_0 and κ on error when L is equal to 1.

In Figure 34 the length of the line segment is set to 1 and with a randomization of ± 5 pixels. When the distortion is significant the SLDC works acceptably and the error is less than 1 pixel. However, when the distortion parameter is small and the line segment is close to the origin the RMSE is higher. The pattern in Figure 34 is also the result of quantisation.
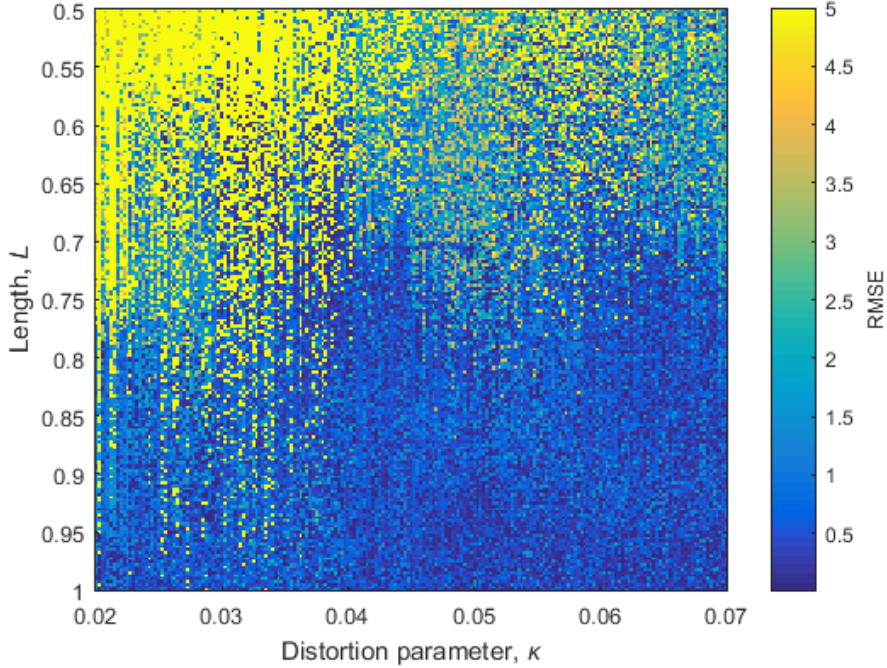
Figure 35: Influence from L and κ on the error when y_0 is equal to 1.

Figure 35 shows the influence for the accuracy from the length of the straight line or the distortion parameter, y_0 is equal to 1 in this simulation and with a randomization of ± 5 pixels. The high error locates at the corner where both L and κ are small. It is clear that when the length of the straight line is shorter than 0.75, the correction method is incapable of correctly estimating the distortion unless the distortion is very serious.

Combing the results of these three plots, the influence from y_0 and κ is similar; when y_0 and κ is small the line will be distorted slightly. The corresponding Hough pattern of a slightly distorted line is hard to analyse, therefore, the error introduced by the correction method is higher. The influence from the length of the line is different from the previous two factors. One reason is from Chapter 3, $\Delta c = \kappa y_0 (L/2)^2$, so the size of the Hough pattern is influenced by the square of length which made it significant compared with those two. Another reason is in the Hough space, points with higher votes correspond to points in image space which are near the symmetry axis of the line segment. The points near the end of the line segment are not taken into account in some cases. Unless the line is very short there will be very slight influence from the length of the line on the accuracy.

From the previous analysis we make following conclusion: for an 800×800 image, the worst case where our method can still work is when the length of the line is equal to 0.75, distortion

parameter is equal to 0.02, and the distance from the line to the origin is equal to 0.75. In other words, our method is more suitable to correct distorted lines located at the edge of the image and the length of that line should be close to the size of the image. In addition, the analysis so far assumes that the original straight line is symmetric about the origin. The analysis of cases where the line is asymmetric will be covered in next section.

5.4.2. Straight Line is Asymmetric about the Origin

In Figure 36, the original straight line in the image space is asymmetric about the distortion centre, and its corresponding pattern in Hough space is unbalanced. The set of the significant points (smile) is also asymmetric (see the red arc) which influences the accuracy of parabola fitting. Because one significant feature of a parabola is its symmetry, without this feature it is hard to provide an accurate fit.
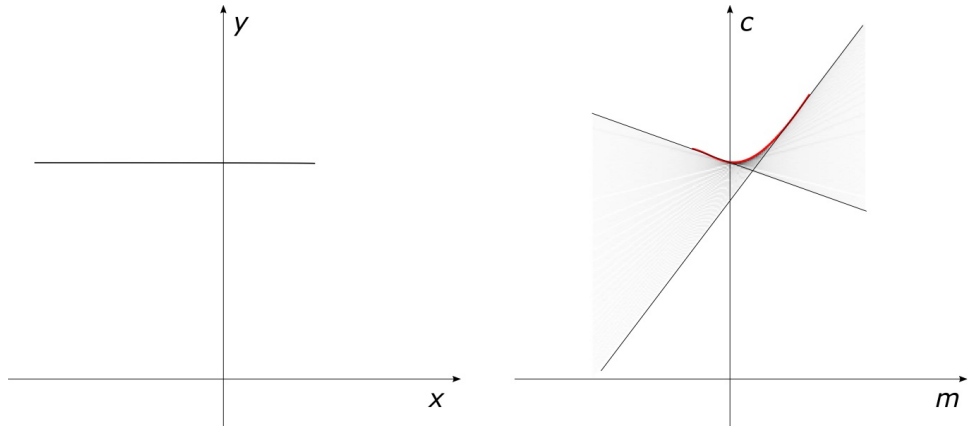
Figure 36: left: the original straight line; right: its corresponding Hough pattern.

The accuracy is also influenced by how much the original straight line is unbalanced. When it is just unbalanced slightly there is a very slight influence on the result. This is because the fit method focuses on points with higher votes, which are located near the symmetric axis. However, when the line segment is not across the symmetric axis or is very short on one side, our method fails to correct the distortion. Attempts to locate the extremum of the parabola have been tried, however, it is impossible to locate the extremum when the original straight line is not across the symmetry axis. Therefore, we conclude that our method is invalid when the original straight line is not approximately asymmetric about the perpendicular line through the image centre.

5.4.3. Line Segment is Tilted

In this section the cases when the original line segment is neither horizontal nor vertical is discussed. In Figure 37, when the line is slightly tilted the corresponding Hough pattern is shifted from its horizontal position. The shifted Hough pattern not influence being able to fit a parabola to it, and not influence estimating the lens distortion parameter, because it not

changes the distortion level within the image. However, this solution only works when the line is tilted slightly, it is because the resolution of the m axis of the original Hough transform changes with slope. This requires further investigation in future works.

Figure 37: left: a horizontal curved line and a tilted curved line; right: Hough patterns
(the blue line represents slope $= 0$).

5.4.4 Moved Lens Distortion Centre

In the previous analysis we assume the centre of the distortion is the centre of the image. However, for real-world images the influence of moving the lens distortion centre cannot be simply ignored. In Figure 38, the left image is a distortion grid and the centre of the distortion is $(50,50)$, the centre image is the corrected image without estimating the lens distortion centre, it is clear that estimating the lens distortion centre is essential for an accurate correction.
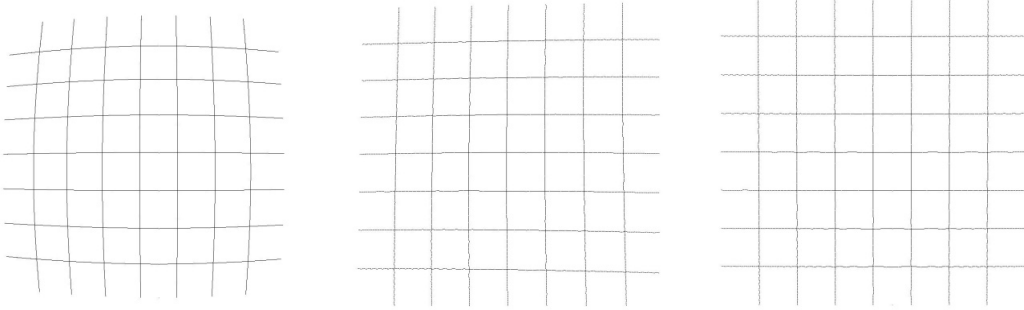
Figure 38: left: the distortion grid with a moved distortion centre; centre: the corrected image without estimating the distortion centre; right: the corrected image with estimated distortion centre.

However, from our experience it is impossible to estimate the lens distortion centre by analysing a single Hough pattern. Instead we provide a way to estimate the distortion centre from a set of parallel lines, which require the image contains a grid or a checkboard. As outlined in Chapter 3, the shape of Hough pattern is influenced by the distance from the original line to the distortion centre (y_0). Any line through the distortion centre remains straight, and its corresponding Hough pattern appears with a single significant point. The 'vote' received by this point is equal to the length of the line. However, when the line segment is away from the distortion centre, there is more distortion and the corresponding Hough pattern is blurred. If we detected the most

significant point in the Hough pattern (the point which highest vote), it receives fewer votes compared with the same length line near the centre. In other works, the votes received by the most significant point in a Hough pattern decreases when the pattern is away from the centre.

Therefore, for a group of parallel lines, by locating the most significant point of each Hough pattern and analysing the 'vote' received by each most significant point it is possible to estimate the lens distortion centre. The vertical and horizontal centre should be estimated separately. Figure 39 shows an example of estimating the horizontal lens distortion centre. In the left of Figure 39 are the detected significant points from a grid. We collect both the number of votes and the distance from the image centre of each point. Then a Gaussian plot is fitted to the significant points from each pattern, the coordinate of the horizontal centre should be located at the peak of the Gaussian plot. The vertical lens distortion centre can be estimated by the same process. When the distortion centre is estimated, a more accurate correction can be provided, see the right image in Figure 39.
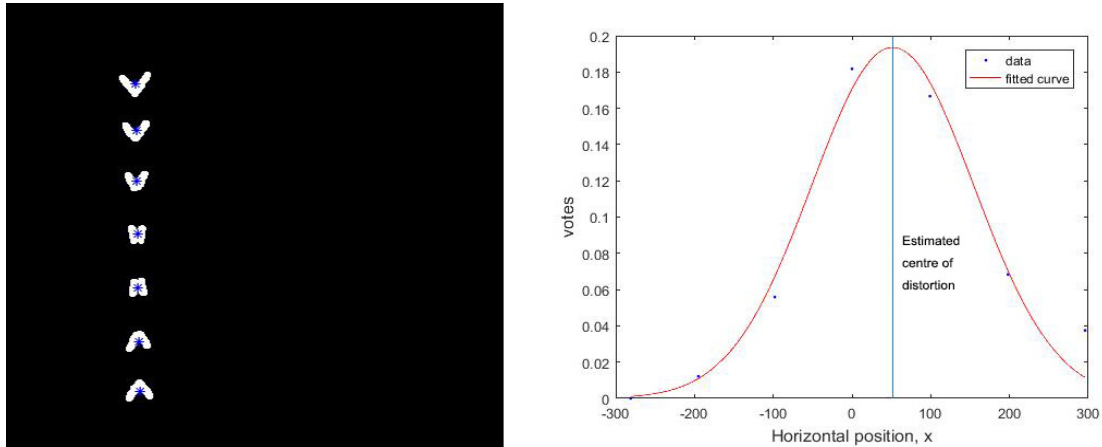
Figure 39: left: a group of Hough patterns and detected most significant points; right: the fitted Gaussian curve.

However, this distortion centre estimation method requires the image to contain a group of straight lines. A more general robust method will be proposed in future works.

5.5. High-Resolution Hough Transform

As described earlier, the error of the SLDC mainly comes from the quantisation during the Hough transform. A higher resolution Hough domain can limit the influence of rounding. In the previous section, the bin resolution in Hough domain was 1131×628, corresponding to an intercept resolution of 1 pixel and a slope resolution of 0.05. To test the effect of a high-resolution Hough domain, we double the bin resolution to 2262×1256. A higher slope resolution can provide more data points for parabola fitting. And for the intercept, in the high-resolution Hough domain has 0.5 pixels per bin. From the density analysis, the high intercept resolution limits the error to 0.5 pixels for each slope. Table 3 compares the results from the

normal resolution Hough transform and the high-resolution transform when correcting the same distorted line.

Lens distortion parameter	0.02	0.03	0.04	0.05	0.06	0.07	0.08	0.09	0.1
Error in $\kappa \times 10^{-3}$ (Normal)	1.34	0.93	0.21	0.52	0.87	1.73	1.21	2.14	1.01
Error in $\kappa \times 10^{-3}$ (High)	0.48	0.96	1.33	0.53	1.15	1.64	0.21	1.5	1.84

(a)

Lens distortion parameter	0.011	0.012	0.013	0.014	0.015	0.016	0.017	0.018	0.019
Error in $\kappa \times 10^{-3}$ (Normal)	4.43	5.75	1.58	5.04	1.12	0.29	0.43	0.21	0.18
Error in $\kappa \times 10^{-3}$ (High)	0.63	1.10	0.91	0.11	0.15	0.33	0.15	0.71	0.55

(b)

Table 3: Accuracy between the normal and high-resolution Hough space.
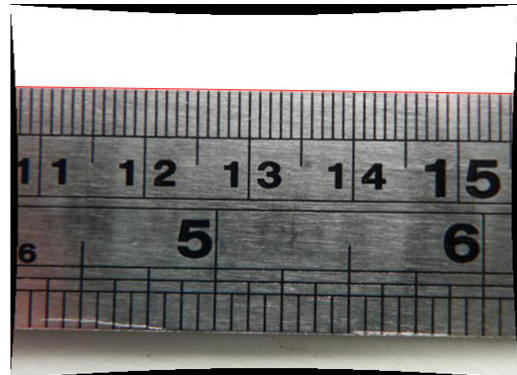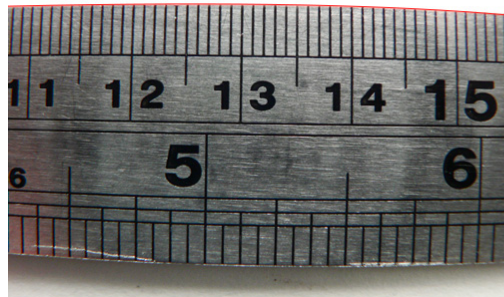
When the distortion is significant both methods achieve similar accuracy. In Table 3 (b), when the lens distortion becomes slight, the normal resolution method fails to correct it, while the High-resolution method remains acceptable. Therefore, it is possible to increase the accuracy by mapping the original image into a higher resolution Hough domain when the lens distortion is slight.

This chapter has demonstrated that the bin quantization while calculating the Hough transform brings the most error in the SLDC. By analysing the length and position of the line segment and the distortion level, the SLDC is suitable to correct distorted images with a long reference line segment located at the edge of the image. In the next chapter example of correcting real-world images will be presented.
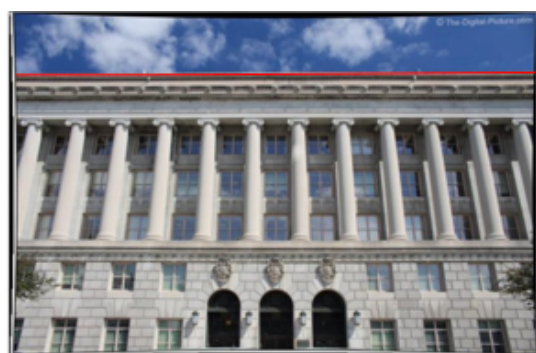
Chapter 6 Results and Discussion

6.1. Real World Image
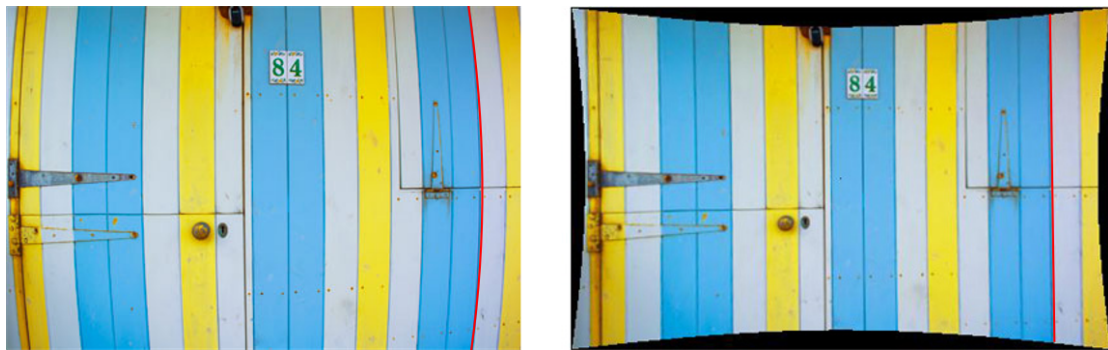
In order to show how the SLDC works with real world images, a group of distorted images have been tested; those images are from the Internet. Images are processed based on the steps described in Chapter 4, and the original image (left) and corrected image (right) are shown in Figure 40. Edges used as the reference to correct distortion have been highlighted in red. The original distortion parameter and the 'true' position of the edge are unknown, therefore we chose to analyse the accuracy by assessing the straightness of corrected edges. The straightness is measured by fitting a straight line to the chosen edge (those edges also have been highlighted) and calculating the residual RMSE. The RMSEs are shown in Table 4. When correcting, the distortion centre is assumed to be the centre of the image. We also compared the correction accuracy of the SLDC with our previous method (Chang, et al, 2017), the result also shown in Table 4.

(a) (https://www.pinterest.nz/imtiazudes/south-american-food-brazilian-cuisines/?lp=true)

(b) (https://ivanero123.wordpress.com/2014/04/13/canon-ef-s-18-55mm-f3-5-5-6-is-stm-lens-review/)

(c) (https://www.practicalphotography.com/camera-advice/questions-and-answers/what-is-lens-distortion)

(d) (http://www.real-me.net/ddyer/photo/wideangle.html)

(e) (https://www.epaperpress.com/ptlens/distortion.html)

(f) (https://www.bdcuniversity.com/art-and-science-rendering-visualization-sells-architecture)

(g) (https://www.epaperpress.com/ptlens/lensCorrect.html)

(h) (https://forum.dji.com/thread-15690-1-1.html)

(i) (https://www.dpreview.com/forums/post/54638813)

(j) (https://havecamerawilltravel.com/photographer/olympus-tough-fisheye-lens/)

Figure 40: left: distorted images; right: corrected images. The edge which was used as the reference to correct the distortion and measure the straightness is highlighted.

Image	a	b	c	d	e	f	g	h	i	j
RMSE of SLDC	0.67	0.49	0.32	0.51	0.54	0.13	0.89	0.59	0.65	1.89
RMSE of previous method	0.66	0.59	0.51	0.65	1.35	0.53	2.18	0.70	0.66	1.78

Table 4: The RMSE when fitting a straight line to the corrected edges.

In Figure 40 (a-i), the distortion has been removed effectively and the RMSE when fitting a straight line to the corrected edge is low. Spatial quantisation in image space makes the edge appear with a series of pixel steps, which increases the RMSE. With uniform quantisation error, the expected RMSE of a perfectly straight line is $\sqrt{\frac{1}{12}} = 0.29$. Our method shows encouraging results when correcting images with moderate distortion.

In Figure 40 (j), the reference is the edge of the upper wall, which is slanted. Even from subjective perspective, most of the distortion has been removed from the image (j) although the corrected edge is waved rather than straight. As a result, the RMSE of the reference edge is higher than other images. The reason is the distortion centre of this image not locates at the centre of the image, instead it is offset to the right side. Using an incorrect centre of distortion made the corrected edge appear waved.

(http://www.joeraasch.com/lens-distortion-workflow-in-nuke/)
Figure 41: Correcting image with serious distortion

On the left of Figure 41 the image is seriously distorted by the wide angle lens. We used the right window edge as the reference to correct the distortion. On the right of Figure 41, the centre of the image is over corrected, while the distortion parameter is insufficient to correct the distortion at the edge of the image. The serious distortion caused by wide angle lens or fisheye lens cannot be accurately modelled by a simple fist order model. Only using one edge as reference also limits the number of parameters which can be estimated.

6.2. Accuracy Comparison with the Previous Method

In previous research we proposed a feature point-based method (described in chapter 3). This section compares the accuracy between the SLDC and the previous method. First an

800×800 undistorted original grid is distorted by given κ, then the distortion is corrected by these two methods, the error is measured by the RMSE. Table 5 compares the RMSE of these two methods with different distortion parameters. Figure 42, shows grids before and after correction when $\kappa = 0.01$.

| (a) | (b) | (c) | (d) |
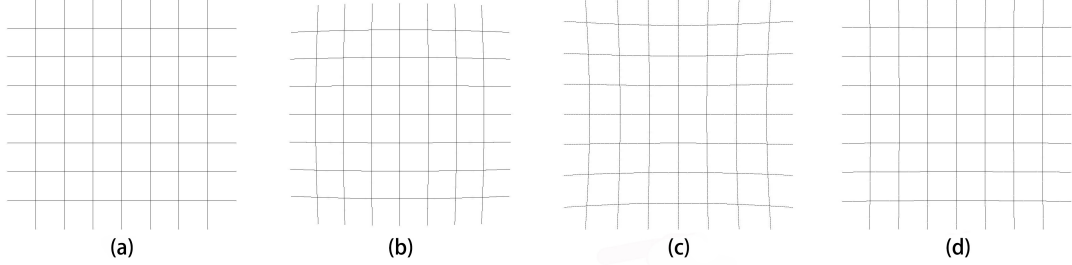
Figure 42: (a) is the undistorted grid; (b) is the distorted grid; (c) is the correction result of the previous method; (d) is the correction result of the SLDC.

Kappa	0.01	0.02	0.03	0.04	0.05	0.06
RMSE of previous method	5.06	8.50	1.07	2.08	1.14	0.47
RMSE of SLDC	0.53	0.85	0.65	0.49	0.29	0.18

Table 5: Comparison the accuracy between the previous method and the 'smile' based method

It is clear that the SLDC shows a higher accuracy than the previous feature point based method, especially when the distortion is slight. In Table 4, (e) and (g) the higher RMSE of the previous method are the result of over correction with inaccurately estimated distortion parameter. Compare with the other images, the distortion within (e) and (g) is slight, therefore we make this conclusion that the SLDC is better than the previous method especially when the distortion is slight.

Inherently, the 'smile' based approach is more accurate than the feature point based method for three main reasons.

I. The 'smile' receives many votes, making it easier to detect and locate.

II. By fitting a smooth curve to the smile, the effects of quantisation and noise can be significantly reduced. It also enables the slope to be calculated more accurately.

III. By using a larger number of curve points to estimate the lens distortion parameter, the effects of noise (including quantisation) can be further reduced.

6.3. Discussion

6.3.1. The advantage of the SLDC

The first advantage of the 'smile' based correction method is that it only needs some line segment detectable in the image scene, which frees it from needing a calibration grid. Any straight edge within the scene can be used to estimate the distortion. Second, this method is independent of distortion model, since the Hough transform and curved line reconstruction are all actually independent of the distortion model. When the curved line is reconstructed any distortion model could be used. In this thesis, we chose an approximation forward model to make the analysis be consistent, but when correcting the distortion a reverse model is also suitable.

6.3.2. Contribution to Other Correction Method

Besides lens distortion correction, by analysing the 'smile' within Hough space, the SLDC provides a curve detection method. Unlike other curve detection methods which locate the curve in image space, the SLDC works by rebuilding the curve from Hough space potentially gaining the advantage of the noise immunity inherent in the Hough transform. Once the curve line is detected, it can be used as an initial step for many correction methods. Bailey (2002) developed a distortion correction method by fitting a parabola to the curved line. Assuming the expression of the parabola is $y = ax^2 + bx + c$, the first order lens distortion coefficient was derived as:

$$\kappa = \frac{-a}{c(3ac + 3b^2 + 1)} \tag{51}$$

Figure 43: Left: distorted image; Right: corrected image by Bailey's method with our reconstructed curved line.

Figure 43 shows the corrected image by using the reconstructed curve as the reference and estimating the distortion parameter from equation (51). Most of the distortion has been removed

and the RMSE when fitting a straight line to the corrected edge of the bookcase is 0.4425. In this experiment the 'smile' detection method has successfully been the initial curve detection method.

Chapter 7 Conclusion and Future Works

7.1. Conclusion

This thesis proposed a lens distortion correction method (SLDC) based on analysing the shape of patterns in the Hough transform space. Different from existing line-based lens distortion correction methods which require line detection as an initial step, the SLDC works by reconstructing the distorted line from the significant points on the Hough pattern, then estimates the distortion parameter by fitting the reconstructed curved line into a straight line and minimising the RMSE. The SLDC only requires some linear features to be visible in image space. Except for this, the SLDC requires no assumptions such as need for a calibration grid. The SLDC is also independent of distortion model, since the Hough transform and curved line reconstruction are all actually independent of the distortion model. When the curved line is reconstructed any distortion model could be used. From both simulation and correcting real world images, the SLDC provides encouraging results, the RMSE when fitting a straight line to the corrected edge is less than 1 pixel. The SLDC also provides a curve detection method for other applications by reconstructing the curved line.

7.2. Suggestions for Future Work

7.2.1. Analyse Multiple Hough Patterns

In this research we demonstrate that the distortion parameters can be estimated by analysing only one Hough 'smile' pattern. This limits the number of parameters which can be estimated, and furthermore limits the distortion model which can be used. Analysing multiple Hough patterns gives more independent data that can be used to increase the order of polynomial model which can be measured. This will increase the accuracy when correcting complex and serious distortion like the distortion caused by fish-eye lenses. Measuring multiple Hough pattern also provides an opportunity to increase the accuracy when estimating the distortion coefficient by effectively averaging the results from multiple 'smiles'. Besides, measuring multiple Hough pattern also provides an opportunity to estimate the distortion centre.

7.2.2. Using the standard Hough Transform

Unlike the original Hough transform, in the standard Hough transform space the angle resolution is uniform. It can bring convenience to the correction when the line segment is not horizontal or vertical. The standard Hough transform also has advantage that it does not require measuring horizontal or vertical edges separately. Therefore, it is necessary to investigate the

effects that the sinusoidal traces of the standard Hough transform would have on the smile pattern, and how these can be used to reconstruct the curved line.

8.0. References

Ahmed, M., & Farag, A. (2005). "Nonmetric calibration of camera lens distortion: differential methods and robust estimation". *IEEE Transactions on Image Processing*, 14(8), 1215-1230.

Alemán-Flores, M., Alvarez, L., Gomez, L., & Santana-Cedrés, D. (2014a). "Automatic lens distortion correction using one-parameter division models". *Image Processing On Line*, 4, 327-343.

Alemán-Flores, M., Alvarez, L., Gomez, L., & Santana-Cedrés, D. (2014b). "Line detection in images showing significant lens distortion and application to distortion correction". *Pattern Recognition Letters*, 36, 261-271.

Alvarez, L., Gómez, L., & Sendra, J. R. (2009). "An algebraic approach to lens distortion by line rectification". *Journal of Mathematical Imaging and Vision*, 35(1), 36-50.

Bacakoglu, H., & Kamel, M. S. (1997). "A three-step camera calibration method". *IEEE Transactions on Instrumentation and Measurement*, 46(5), 1165-1172.

Bailey, D. G. (2002). "A new approach to lens distortion correction". *Proceedings of Image and Vision Computing New Zealand,* 59-64.

Barreto, J. P., & Daniilidis, K. (2005). "Fundamental matrix for cameras with radial distortion". in *Computer Vision*, 625-632.

Basu, A., & Licardie, S. (1995). "Alternative models for fish-eye lenses". *Pattern Recognition Letters*, 16(4), 433-441.

Beyer, H. A. (1992). "Accurate calibration of CCD-cameras". in *Computer Vision and Pattern Recognition,* 96-101.

Bukhari, F., & Dailey, M. N. (2010). "Robust radial distortion from a single image". in *International Symposium on Visual Computing*, *Advances in Visual Computing. ISVC 2010. LNCS vol* 6454. 11-20. *Springer*.

Cai, J., & Miklavcic, S. (2013). "Automatic curve selection for lens distortion correction using Hough transform energy". in *Applications of Computer Vision*, 455-460.

Canny, J. (1986). "A computational approach to edge detection", *IEEE Transactions on Pattern Analysis and Machine Intelligence*, 8(6), 679-698 .

Chang, Y., Bailey, D. G., & Le Moan, S. (2017). "Lens distortion correction by analysing the shape of peaks in Hough transform space". in *Proceedings Image and Vision Computing New Zealand*.

Cucchiara, R., & Filicori, F. (1998). "The vector-gradient Hough transform". *IEEE Transactions on Pattern Analysis and Machine Intelligence*, 20(7), 746-750.

Cucchiara, R., Grana, C., Prati, A., & Vezzani, R. (2003). "A Hough transform-based method for radial lens distortion correction". in *12th International Conference on Image Analysis and Processing*, 182-187.

Duane, C. B. (1971). "Close-range camera calibration". *Photogrammetric Engineering*, 37(8), 855-866.

Faugeras, O., & Toscani, G. (1987). "Structure from motion using the reconstruction and reprojection technique". in *IEEE Workshop on Computer Vision*, 345.

Fernandes, L. A., & Oliveira, M. M. (2008). Real-time line detection through an improved Hough transform voting scheme. *Pattern Recognition*, *41*(1), 299-314.

Frederic, D., & Olivier, F. (1995). "Automatic calibration and removal of distortion from scenes of structured environments". in *Investigative and Trial Image Processing*, *SPIE Vol.* 2567, 62-73.

Frederic, D., & Olivier, F. (2001). "Straight lines have to be straight". *Machine Vision and Applications*, 13(1), 14-24.

Fitzgibbon, A. W. (2001). "Simultaneous linear estimation of multiple view geometry and lens distortion". in *IEEE Computer Society Conference on Computer Vision and Pattern Recognition*.

Furukawa, Y., & Shinagawa, Y. (2003). "Accurate and robust line segment extraction by analyzing distribution around peaks in Hough space". *Computer Vision and Image Understanding*, 92(1), 1-25.

Habib, A., & Morgan, M. F. (2003). "Automatic calibration of low-cost digital cameras". *Optical Engineering*, 42(4), 948-956.

Hughes, C., Glavin, M., Jones, E., & Denny, P. (2008). "Review of geometric distortion compensation in fish-eye cameras". in *Irish Signals and Systems Conference.*

Ishii, C., Sudo, Y., & Hashimoto, H. (2003). "An image conversion algorithm from fish eye image to perspective image for human eyes". in *Advanced Intelligent Mechatronics, IEEE/ASME International Conference*, 1009-1014.

Kunina, I., Terekhin, A., Gladilin, S., & Nikolaev, D. (2017). "Blind radial distortion compensation from video using fast Hough transform". in *International Conference on Robotics and Machine Vision*.

Lee, T.Y., Chang, T.S., Lai, S.H., Liu, K.C., & Wu, H.S. (2011). "Wide-angle distortion correction by Hough transform and gradient estimation". in *Visual Communications and Image Processing* (VCIP), 1-4.

Lee, T.Y., Chang, T.S., Wei, C.H., Lai, S.H., Liu, K.C., & Wu, H.-S. (2013). "Automatic distortion correction of endoscopic images captured with wide-angle zoom lens". *IEEE Transactions on Biomedical Engineering*, 60(9), 2603-2613.

Maini, R., & Aggarwal, H. (2009). "Study and comparison of various image edge detection techniques". *International Journal of Image Processing* (IJIP), 3(1), 1-11.

Mallon, J., & Whelan, P. F. (2004). "Precise radial un-distortion of images". In *IEEE Computer Society Conference on Pattern Recognition. ICPR*, 1, 18-21.

Matas, J., Galambos, C., & Kittler, J. (1998). "Progressive probabilistic Hough transform". in *British Machine Vision Conference*.

McGlone, C., Mikhail, E., & Bethel, J. (1980). "Manual of photogrammetry". *American Society for Photogrammetry and Remote Sensing*.

Mohr, R., & Triggs, B. (1996). "Projective geometry for image analysis". in *XVIIIth International Symposium on Photogrammetry & Remote Sensing (ISPRS)*.

Park, J., Byun, S.-C., & Lee, B.-U. (2009). "Lens distortion correction using ideal image coordinates". *IEEE Transactions on Consumer Electronics*, 55(3).

Prescott, B., & McLean, G. (1997). "Line-based correction of radial lens distortion". *Graphical Models and Image Processing*, 59(1), 39-47.

Rafael Gonzalez, C., & Woods, R. (2002). "Digital image processing". *Pearson Education*.

Remondino, F., & Fraser, C. (2006). "Digital camera calibration methods: considerations and comparisons". *International Archives of Photogrammetry, Remote Sensing and Spatial Information Sciences*, 36(5), 266-272.

Rosten, E., & Loveland, R. (2011). "Camera distortion self-calibration using the plumb-line constraint and minimal Hough entropy". *Machine Vision and Applications*, 22(1), 77-85.

Salvi, J., Armangué, X., & Batlle, J. (2002). "A comparative review of camera calibrating methods with accuracy evaluation". *Pattern Recognition*, 35(7), 1617-1635.

Shah, S., & Aggarwal, J. (1996). "Intrinsic parameter calibration procedure for a (high-distortion) fish-eye lens camera with distortion model and accuracy estimation". *Pattern Recognition*, 29(11), 1775-1788.

Song, L., Wu, W., Guo, J., & Li, X. (2013). "Survey on camera calibration technique". in *5th International Conference on Intelligent Human-Machine Systems and Cybernetics (IHMSC)*.

Swaminathan, R., & Nayar, S. K. (2000). "Nonmetric calibration of wide-angle lenses and polycameras". *IEEE Transactions on Pattern Analysis and Machine Intelligence*, 22(10), 1172-1178.

Tsai, R. (1987). "A versatile camera calibration technique for high-accuracy 3D machine vision metrology using off-the-shelf TV cameras and lenses". *IEEE Journal on Robotics and Automation*, 3(4), 323-344.

Wang, A., Qiu, T., & Shao, L. (2009). "A simple method of radial distortion correction with centre of distortion estimation". *Journal of Mathematical Imaging and Vision*, 35(3), 165-172.

Wang, Q., Li, F., & Liu, Z. (2010). "Review on camera calibration". in *Control and Decision Conference (CCDC)*.

Xu, D., Li, Y., & Tan, M. (2006). "Method for calibrating cameras with large lens distortion". *Optical Engineering*, 45(4), 043602.

Zhang, Z. (2000). "A flexible new technique for camera calibration". *IEEE Transactions on Pattern Analysis and Machine Intelligence*, 22(11), 1330-1334.

Zhou, F., Cui, Y., Gao, H., & Wang, Y. (2013). "Line-based camera calibration with lens distortion correction from a single image". *Optics and Lasers in Engineering*, 51(12), 1332-1343.